LBL-35628
UC-331

Lawrence Berkeley Laboratory

UNIVERSITY OF CALIFORNIA

ENERGY & ENVIRONMENT DIVISION

Nickel Hydroxide Electrodes in Reduced-Alkalinity Electrolytes

R.F. Plivelich,* F.R. McLarnon, and E.J. Cairns
(*M.S. Thesis)

April 1994

ENERGY & ENVIRONMENT DIVISION

REFERENCE COPY
Does Not
Circulate
Bldg. 50 Library.
LBL-35628
Copy 1

Prepared for the U.S. Department of Energy under Contract Number DE-AC03-76SF00098

DISCLAIMER

This document was prepared as an account of work sponsored by the United States Government. While this document is believed to contain correct information, neither the United States Government nor any agency thereof, nor the Regents of the University of California, nor any of their employees, makes any warranty, express or implied, or assumes any legal responsibility for the accuracy, completeness, or usefulness of any information, apparatus, product, or process disclosed, or represents that its use would not infringe privately owned rights. Reference herein to any specific commercial product, process, or service by its trade name, trademark, manufacturer, or otherwise, does not necessarily constitute or imply its endorsement, recommendation, or favoring by the United States Government or any agency thereof, or the Regents of the University of California. The views and opinions of authors expressed herein do not necessarily state or reflect those of the United States Government or any agency thereof or the Regents of the University of California.

LBL-35628

NICKEL HYDROXIDE ELECTRODES IN REDUCED-ALKALINITY ELECTROLYTES

by

Robert F. Plivelich, Frank R. McLarnon and Elton J. Cairns

Energy & Environment Division
Lawrence Berkeley Laboratory
University of California
Berkeley, California 94720

April 1994

This work was supported by the Assistant Secretary for Energy Efficiency and Renewable Energy, Office of Transportation Technologies, Electric and Hybrid Propulsion Division of the U.S. Department of Energy under Contract No. DE-AC03-76SF00098.

Table of Contents

Page

List of Tables iv

List of Figures v

Acknowlegements ix

Chapter I
Introduction 1

Chapter II
Background 5

Chapter III
Experimental Apparatus and Methods 15

Chapter IV
Results and Discussion 33

Chapter V
Conclusions and Recommendations 69

Appendix
Preparation and Characterization
of Reference Compounds 72

Bibliography 78

List of Tables

Page

Table 1.1
Selected USABC battery performance criteria 2

Table 1.2
Performance of common battery systems 3

Table 2.1
Unit cell parameters for nickel oxide phases 7

Table 3.1
Preparation or sources of reference compounds 18

Table 3.2
Summary of cycling experiments 32

Table 4.1
Peak identification for β–$Ni(OH)_2$ survey spectrum 36

Table 4.2
Peak identification for ZnO survey spectrum 36

Table 4.3
Reported Ni $2p_{3/2}$ binding energies for β–$Ni(OH)_2$ 55

List of Figures

Page

Figure 2.1
The Bode cycle 5

Figure 3.1
Cycling behavior of a 21 A-h zinc-nickel oxide cell utilizing a reduced-alkalinity electrolyte [49]. 16

Figure 3.2
Photoelectron emission 20

Figure 3.3
Auger electron emission 21

Figure 3.4
Four-point probe method for resistivity measurements. 25

Figure 3.5
Positioning of leads for four-point resistivity measurements 26

Figure 3.6
Schematic of cell used in most cycling experiments. 28

Figure 3.7
Schematic of cell used in cycling with compression. 31

Figure 4.1
Survey photoelectron spectrum of β–$Ni(OH)_2$ 34

Figure 4.2
Survey photoelectron spectrum of ZnO 35

Figure 4.3
Zn $2p_{1/2}$ photoelectron spectra of ZnO and $Zn(OH)_2$ 37

Figure 4.4
Ni $2p_{3/2}$ / $2p_{1/2}$ photoelectron spectrum of β–$Ni(OH)_2$ 38

Page

Figure 4.5
Ni $2p_{3/2}$ photoelectron spectra of β–$Ni(OH)_2$ and β–NiOOH. 39

Figure 4.6
Ni $2p_{3/2}$ photoelectron spectra of α-$Ni(OH)_2$ and β–$Ni(OH)_2$ 41

Figure 4.7
Zn $2p_{3/2}$ photoelectron spectra of α-$(Ni,Zn)(OH)_2$
and $Zn(OH)_2$ (Ni : Zn ratio = 10).....42

Figure 4.8
Zn $2p_{3/2}$ photoelectron spectra of α-$(Ni,Zn)(OH)_2$
and ZnO (Ni : Zn ratio = 1) 43

Figure 4.9
Ni $2p_{3/2}$ photoelectron spectra of α-$(Ni,Zn)(OH)_2$
(Ni : Zn ratio = 10).....44

Figure 4.10
Raman spectra of α–$Ni(OH)_2$ and 1 : 1 α–$(Ni,Zn)(OH)_2$ 45

Figure 4.11
Ni $2p_{3/2}$ spectra of nickel electrode material cycled
in reduced alkalinity electrolyte and β–$Ni(OH)_2$ 48

Figure 4.12
Zn $2p_{3/2}$ spectra of nickel electrode material cycled
carbonate electrolyte and $Zn(OH)_2$ 49

Figure 4.13
Ni $2p_{3/2}$ spectra of nickel electrode material cycled
in reduced alkalinity electrolyte and in standard electrolyte 50

Figure 4.14
Zn $2p_{3/2}$ spectra of nickel electrode material cycled
reduced alkalinity electrolyte and in standard electrolyte 51

Page

Figure 4.15
Zn $2p_{3/2}$ spectra of a nickel hydroxyzincate before and after washing in hot KOH 52

Figure 4.16
Zn $2p_{3/2}$ spectra of nickel electrode material cycled in reduced alkalinity electrolyte, before and after washing in hot KOH 54

Figure 4.17
Cell configuration, and sampling locations for resistivity measurements 58

Figure 4.18
Resistivity variation of nickel electrode Ni A at four locations 59

Figure 4.19
Resistivity variation of nickel electrodes through the cell pack. 60

Figure 4.20
Optical micrograph of uncycled nickel electrode material. 62

Figure 4.21
Optical micrograph of cycled nickel electrode material 63

Figure 4.22
Influence of surfactant concentration on discharge capacity 66

Figure 4.23
Effect of washing on discharge capacity 67

Figure 4.24
Effect of compression on discharge capacity 68

Figure A.1
X-ray diffraction pattern of β–$Ni(OH)_2$ 74

Figure A.2
X-ray diffraction pattern of α–$Ni(OH)_2$ 75

Page

Figure A.3
X-ray diffraction pattern of β–NiOOH.....75

Figure A.4
X-ray diffraction pattern of a nickel hydroxyzincate
with a nickel-zinc ratio of 1:1.....76

Figure A.5
X-ray diffraction pattern of a nickel hydroxyzincate
with a nickel-zinc ratio of 10:1.....76

Figure A.6
X-ray diffraction pattern of $Zn(OH)_2$.....77

Figure A.7
X-ray diffraction pattern of ZnO.....77

Acknowledgements

I would like to express my appreciation to F. R. McLarnon and E. J. Cairns for their patient advice and support during the course of this work. Without their assistance, it wouldn't have been possible. For their help on some of the electrochemical fundamentals (e.g. "What is, and how do you use, a reference electrode?"), the contributions of K. Striebel, T. Adler and J. Rudnicki were invaluable. All those who contributed in some way to this work are, of course, too numerous to mention, but special thanks goes to D. Littlejohn and M. Odziemkowski for their assistance with the Raman spectroscopy. The helpful reviews of this work by C. W. Tobias and J. W. Evans are also gratefully recognized.

This work was supported by the Assistant Secretary for Energy Efficiency and Renewable Energy, Office of Transportation Technologies, Electric and Hybrid Propulsion Division of the U.S. Department of Energy under Contract No. DE-AC03-76SF00098.

Chapter I: Introduction

The development of better-performing battery systems can help meet some of the environmental and economic challenges facing our society. It is worthwhile to examine such considerations before beginning a technical discussion. Recently, in response to various environmental concerns, a law was passed by the California legislature mandating the sale of so-called zero-emission vehicles. These vehicles would almost certainly be powered electrically, with batteries as the power source. On a national level, the U. S. Advanced Battery Consortium (USABC), a partnership comprised of American companies, the U. S. Department of Energy, and the Electric Power Research Institute, was recently created with the goal to develop high-performance batteries for use in electric vehicles. Table 1.1 lists some of the key battery performance goals. One should note that to date there is no single battery system that can completely meet all of these criteria.

One can consider the markets for batteries. George [2] has estimated that worldwide (non-communist) battery production amounted to about $ 17 billion in 1988, of which $ 4.7 billion was in the United States. Since at that time roughly one-half of the world's population was under communist control, the potential global market size is certainly significantly larger. The potential market for electric-vehicle batteries is also quite large. By making a few plausible assumptions, one can estimate the potential market for batteries in electric vehicle applications [3]. The American automobile fleet presently numbers about 180 million vehicles,

Table 1.1: Selected USABC battery performance criteria [1]

Performance Goal	Mid-term	Long-term
Specific Energy (Wh/kg)	80	200
Volumetric Energy Density (Wh/l)	135	300
Specific Power(W/kg)	150	400
Volumetric Power Density (W/l)	250	600
Cycle Life (charge/discharge cycles)	600	1000
Maintenance	zero	zero

about 1/8th of which are in California. Assuming a 10% turnover of autos per year, and about $5,000 per auto for batteries, one can project an upper estimate of over $10 billion for the size of the battery market for electric vehicles in California alone, and about $90 billion in the United States. On a global scale, the potentially huge size of the market can be appreciated. It should be noted, however, that not all gasoline-powered vehicles are likely to be replaced in the forseeable future by electric cars. It is also likely that more than one battery system would be adopted depending on the vehicle's intended service, just as there are differing requirements of gasoline and diesel engines depending on the vehicle type.

As Table 1.2 suggests, zinc/nickel oxide batteries are attractive in terms of specific energy and specific power when compared with other common battery systems. In particular, one should note the advantages

Table 1.2: Performance of common battery systems [4]

Cell Type	E^0 (V)	Specific Energy E (Wh/kg)	Specific Power P (W/kg)	Cycle Life
lead/acid	2.095	35-40 at P=10	100-200 at E=10	100-1000
hydrogen/ nickel oxide	1.4	60 at P=20	60 at E=50	1000-2000 at P=20, 60% DOD
zinc/ nickel oxide	1.7	55-75 at P=10	> 200 at E=35	> 500 at P=25-50, 100% DOD
iron/ nickel oxide	1.2	40-60 at P=10	70-150 at E=10	2000-4000
metal hydride/ nickel oxide	1.2	48-58	> 200	> 500, 100% DOD
zinc/air	1.6	100-120 at P=40	150	< 300
zinc/bromine	1.85	75 at P=20	< 100	200-2000 90-100%DOD
lithium-ion	3.6	80	> 200	> 600, 100% DOD
lithium/polymer	2.76-2.1	150	400	> 100, 80% DOD
sodium/sulfur	2.08-1.7	< 190	< 250 peak	600-2000

when compared with the most well-established system, namely the lead-acid battery. One should also note that zinc/nickel oxide batteries could potentially meet the USABC mid-term criteria for high-performance electric vehicle batteries. Another advantage of the zinc/nickel oxide system is the relatively low toxicity of its component materials (especially as compared to cadmium/nickel oxide), with disposal of spent battery materials an important consideration for widespread EV operation. A primary flaw of the zinc/nickel oxide system, as Table 1.2 indicates, is its relatively short cycle life. Most research efforts concerning zinc/nickel oxide batteries have been aimed at increasing the cycle life.

Purpose and organization of this work

This document is an account of work examining the possible causes of observed capacity loss of nickel hydroxide electrodes used in zinc/nickel oxide cells which incorporated novel electrolytes intended to extend the cell's cycle life. A brief introduction to the electrochemistry of the nickel hydroxide electrode, and aspects of zinc/nickel oxide battery technology will be given in the next chapter. Subsequent chapters will outline the various experimental techniques used, and experimental results obtained. The final chapter will present conclusions and recommendations based on this work.

Chapter II: Background

The zinc/nickel oxide system is a rather complex one, with coupling occurring among the processes that ultimately determine the lifetime of each electrode. We will first briefly consider some of the fundamental aspects of nickel electrodes and zinc electrodes, and then outline the approach taken here to clarify the capacity-decline modes of this system.

Introduction to the nickel hydroxide electrode

Early work aimed at characterizing the system was done by Glemser and Einerhand [5]. Through wet-chemical synthesis, and x-ray diffraction analysis, they did much to elucidate the various nickel-oxygen compounds that arise. Later work by Bode and co-workers [6] provided a description of the nickel hydroxide system in alkaline media which is accepted to this day. In honor of Bode, this framework is known as the Bode cycle.

As Figure 2.1 indicates, Bode identified four primary phases involved in the electrochemistry of nickel hydroxide. A brief description of these phases is in order.

Figure 2.1: The Bode cycle

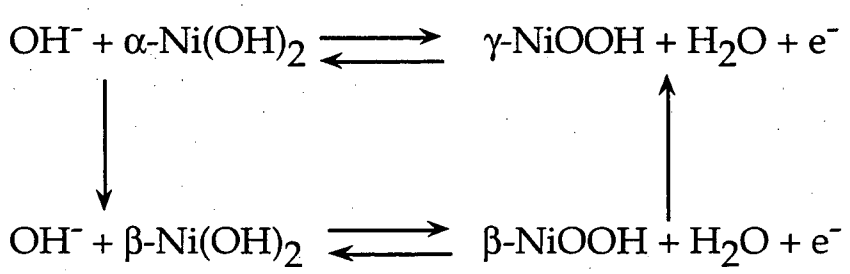

β–nickel (II) hydroxide

This is the form of nickel oxide encountered when one has a discharged nickel electrode under normal conditions. It belongs to the hexagonal crystal system, with a brucite (or $Mg(OH)_2$) structure. Table 2.1 lists the unit cell parameters for this and other nickel oxide phases of interest. One can produce this material in a highly crystalline form by precipitation with base from a nickel nitrate solution followed by hydrothermal treatment [7]. The form of β-$Ni(OH)_2$ encountered in electrochemical systems is notable for its higher surface area and greater disorder than the crystalline chemically-prepared form [8].

β–nickel (III) oxyhydroxide

This phase is obtained when one charges β–nickel (II) hydroxide. It largely retains the brucite structure, but has a slightly greater intersheet distance than β-$Ni(OH)_2$, as indicated by the "c" unit cell parameter in the hexagonal system. This expansion of the intersheet distance is apparently due to absorption of electrolyte and water.

α–nickel (II) hydroxide

This particular form is obtained early in cycle life. It is characterized by a high degree of hydration [9], which is reflected in its greater intersheet distancce relative to β-$Ni(OH)_2$. The structure belongs to the hexagonal system, but with a great degree of disorder present. The layered sheets of this material exhibit no preferred orientation (i.e., they are turbostratic, similar to some forms of carbon blacks.) Water is both absorbed and intercalated between the sheets.. It is also unstable in either neutral or alkaline solution, eventually converting into the β-nickel (II) hydroxide

form. This ageing is thought to occur by an Ostwald ripening process, with smaller particles of α–$Ni(OH)_2$ dissolving, and larger particles of β-$Ni(OH)_2$ crystallizing [10].

<u>γ–nickel (III) oxyhydroxide</u>

This form is obtained by overcharge from β-nickel (III) oxyhydroxide, and by charging from the α-nickel (II) hydroxide form [7]. There are several crystal forms of this material reported; the one reported by Glemser and Einerhand [5] belongs to the rhombohedral system. It too is a hydrated compound, with intercalated water present. It is thought that γ-NiOOH has a higher bulk oxidation state than does β-NiOOH. Therefore, the α–$Ni(OH)_2$ to γ-NiOOH charging reaction would be preferable from a cell-performance point of view relative to the β-$Ni(OH)_2$ to β-NiOOH charging reaction.

Table 2.1 Unit cell parameters for nickel oxide phases [7]

Phase	**Structure**	**a (Å)**	**c (Å)**
β-$Ni(OH)_2$	Hexagonal	3.1	4.6
β-NiOOH	Hexagonal	2.82	4.85
α-$Ni(OH)_2$	Hexagonal	3.1	8.5
γ-NiOOH	Rhombohedral	2.82	20.65

One should keep in mind that the notation is a general crystallographic one. The materials that exist in the Bode cycle are non-stoichiometric. Within a given class, there may be variations in oxidation

state and/or degree of hydration. For example, it is possible to synthesize a whole spectrum of α-nickel (II) hydroxides [9]. They will be characterized by similar crystalline structures, but differing degrees of hydration. Similar comments apply to the other three phases of the Bode cycle.

There are several methods to prepare nickel hydroxide electrodes for use in batteries, with the performance characteristics of the cell being greatly influenced by this choice. The usual method is to first prepare a porous nickel structure, typically by sintering carbonyl nickel powder onto a metal grid which serves as a current collector. The nickel hydroxide active material is deposited in the pores [11] by precipitation, caused to occur either chemically or electrochemically. In the chemical method, one simply fills the pores with a nickel salt solution (typically nickel nitrate), and then dips the filled electrode into an alkaline solution, which precipitates the nickel hydroxide [e. g. 12]. This process is repeated until the desired loading of $Ni(OH)_2$ is attained. In the electrochemical method, the sintered nickel structure is placed in a warm aqueous bath containing nickel nitrate. The electrode is then cathodically polarized, with the result that nickel hydroxide is precipitated. This process is rather complex, the subject of numerous studies [e.g. 13], with side reactions involving the production of ammonia and other species. One should also note that the porous sintered nickel plaque is quite heavy and expensive. Currently there are research efforts aimed at replacing this plaque with lighter-weight and less-costly nickel foams and felts, and various nickel-plated polymer substrates.

Several causes of capacity loss in nickel hydroxide electrodes have been postulated. Perhaps the most common, and the least well- quantified

process, is the loss of wetting of the electrode pores during cycling. When the end of charge of a nickel electrode is approached, oxygen evolution begins to compete with the nickel oxidation reaction [14]. The gas can presumably force the electrolyte from pores, thereby drying the electrode, and causing a loss of capacity. The oxygen evolution reaction on metallic nickel, nickel oxides and hydroxides, and other materials has been studied by many investigators [14-18], and will not be considered further in this work.

Another mode of capacity loss is thought to be mechanical damage of the sintered nickel current collector during cycling, with accompanying isolation of Ni active material from the current-collecting structure. In the early 1980s Fritts addressed this issue [19]. In one study, by manipulating the preparation conditions of a nickel electrode, he found that he could induce the formation of blisters within the electrode during cycling. The blistering, he concluded, was caused by the formation of macropores in the electrode, which served as collection points for oxygen evolved during charging. These macropores, in turn, were thought to be caused by a gradient in the rigidity of the sintered nickel substrate in the direction away from the current-collecting grid. No blistering was observed when oxygen evolution was avoided. In a later study [20], Fritts found that the conductivity loss of a sintered nickel electrode generally followed the capacity loss of the electrode. He then concluded that this conductivity loss reflected the formation of electrically isolated islands within the electrode. It should be mentioned that the cadmium/nickel oxide system was studied by Fritts, and not the zinc/nickel oxide system as considered in this work. A later modeling study by Lanzi and Landau [21] qualitatively supported the conclusions of Fritts.

Another postulated capacity-loss mechanism is the formation of low-conductivity layers during discharge of the electrode. It is known that the conductivity of NiOOH is approximately three orders of magnitude greater than that of $Ni(OH)_2$ [22]. The formation of a layer of relatively non-conductive $Ni(OH)_2$ near the conductive metallic substrate can presumably lead to capacity loss by forcing a large fraction of the current to travel through the non-conductive layer [21, 23]. One can consider this to be related to the sinter-fracture mode, in that current is being forced to travel through paths of high resistivity.

A mode of capacity loss associated specifically with zinc/nickel oxide cells is the precipitation of ZnO or $Zn(OH)_2$ in the pores of the nickel oxide electrode [24] . This process is thought to reduce the active area accessible to the electrolyte, thereby decreasing the electrode's capacity. In one case, it was found possible to recover the capacity of failing nickel electrodes in a zinc/nickel oxide cell by washing in hot 10 N KOH, although published details were sparse [25]. Formation of "nickel hydroxyzincates" [6] have also been suspected of causing nickel electrode capacity loss in zinc/nickel oxide cells [26, 27].

An argument against ZnO precipitation or electrochemically inactive zinc-nickel oxide compounds is the observation that most zinc transfer to the nickel electrode occurs early in the first few cycles, whereas capacity loss occurs more gradually [28, 29], over tens or hundreds of cycles. Because the zinc electrode is typically taken as the life-limiting electrode of zinc/nickel oxide cells, little work has been done in examining the degradation modes of nickel electrodes in such cells.

There are several steps that can be taken to improve the performance of nickel hydroxide electrodes. One approach is to place additives in the electrode bulk. Cobalt, in concentrations of approximately 5 to 10 percent, is universally incorporated into nickel oxide electrodes for battery applications. There is evidence that Co improves the conductivity of the nickel active material [30], although there are claims that this is only so in the presence of lithium ions in the electrolyte [31]. Voltammetric studies provide evidence that Co improves the reversibility of the nickel redox reactions as well [32]. Other metal ions, such as zinc and manganese, have also been shown to improve electrochemical performance when co-precipitated during preparation of the nickel hydroxide electrode [32, 33, 34].

Another approach for performance improvement is to place additives into the electrolyte. Lithium hydroxide, in concentrations of about 1M, is typically used. Lithium has been shown to increase the overpotential for oxygen evolution [31], and is also thought to help improve the conductivity of the active material [31]. Recent work [35] suggests that Li^+ intercalates into the bulk of the electrode.

Another additive which has been used in the electrolyte is carbonate. Voltammetric work suggests that it improves the reversibility of the Ni^{2+} to Ni^{3+} electrode reaction [36, 37]. It is also known, however, that carbonate will lower the overpotential for oxygen evolution on nickel [37]. An enhanced rate of oxygen evolution may accelerate the mechanical degradation of the sintered nickel current collector. The benefits of carbonate usage with nickel electrodes are thus somewhat unclear.

Introduction to the alkaline zinc electrode

The stoichiometry of zinc oxidation in alkaline solutions can be written as follows [38]:

$$Zn + 4(OH)^- \rightarrow Zn(OH)_4^{2-} + 2e^- \qquad (1)$$

$$Zn(OH)_4^{2-} \rightarrow ZnO + 2OH^- + H_2O \qquad (2)$$

Metallic zinc is oxidized to the zincate ion, which may precipitate to yield either zinc oxide or zinc hydroxide (not shown). Electrolytically, one can achieve a large degree of supersaturation. It should be noted that supersaturated zincate solutions are metastable, with times of up to a year needed to attain the equilibrium saturation value of zincate concentration [39]. It has been suggested that the precipitation of zinc oxide occurs in a two-path process, one path being a homogeneous reaction in solution, and the other a heterogeneous one, wherein solid zinc oxide particles serve as a catalyst for further precipitation [40, 41]. Two different morphologies of zinc oxide precipitates have been observed. One is a loosely-adhering deposit, speculated to be $Zn(OH)_2$, and is referred to as a "Type I" deposit. The other type of precipitate, "Type II", is thought to be a denser, passivating layer of ZnO [42].

Zinc electrodes are commonly used in both primary (non-rechargeable) and secondary alkaline battery systems. There exist, however, several problems with the secondary alkaline zinc electrode [42]. One problem is dendrite formation leading to electrical short-circuiting of cells. Another is the redistribution of zinc after repeated charge-discharge cycles. This is known as "shape change", and is a result of the high solubility of zinc oxide (or zinc hydroxide) in strong alkaline electrolytes. As with the nickel electrode, another factor which can induce capacity loss

is the drying of the electrode, which is related to gas evolution phenomena.

There are steps one can take to improve the cycle-life performance of zinc electrodes. For example, to mitigate the dendrite problem, one can use various separator materials of smaller pore size [42]. A sealed-cell configuration also lessens this problem. In alkaline zinc cells, oxygen evolved during the overcharge of the positive electrode is thought to oxidize any zinc dendrites that are formed on the negative electrode [18]. One can include surfactants in the electrolyte to improve the electrode's wetting properties. An approach that has been tried by many workers, including members of our research group, is to reduce the alkalinity of the electrolyte in an attempt to reduce shape change. Chen, et. al., found that various additives, such as fluorides, borates, and carbonates, reduced shape change in zinc/silver oxide cells, although cell cycle life was not improved [43]. Jain, et al. [44] found that adding $Ca(OH)_2$ to the negative electrode of zinc/nickel oxide cells helped to reduce shape change, presumably by forming less soluble calcium zincate species. There have also been studies of reducing the KOH concentration in zinc/nickel oxide cells. An early screening study by Thornton and Carlson [45] found that reducing the alkalinity of the electrolyte was indeed effective in reducing the solubility of the zinc electrode. They suggested the use of KF as a supporting electrolyte. A recent study by Adler, et.al. [28], suggests that a combination of reducing KOH concentration, and adding CO_3^{2-} and F^-, both reduces shape change and increases the cycle life of zinc/nickel oxide cells (over 500 cycles in the best case, at 100% DOD.) In this case, a sealed-cell configuration eliminated shorting by dendrites. They reached an unusual situation in which the nickel electrode and not the zinc electrode,

was the cycle-life-limiting component of the cell. The use of borates has also been shown to reduce shape change [46, 47, 48] of zinc electrodes in zinc/nickel oxide cells.

Examining the failure of zinc/nickel oxide cells

As mentioned earlier, the work of Adler et. al. [28] established that by using low-alkalinity electrolytes, it is possible to extend zinc electrode cycle life to the extent that the nickel oxide electrode is the life-limiting component of zinc-nickel oxide cells. This point is reached by the use of modified electrolytes of reduced alkalinity. The approach outlined here will emphasize the examination of mechanical shortcomings as a contributing factor to ultimate capacity loss of the nickel oxide electrodes of zinc/nickel oxide cells cycled in a reduced-alkalinity electrolyte . This investigation addresses three likely causes: 1) reduction of the active surface area with species precipitated from solution (ZnO, $Zn(OH)_2$, or a fluoride or carbonate); 2) conversion of the surface from an active form to an inactive one, by a non-Faradaic reaction with the electrolyte (nickel hydroxyzincate formation); and 3) damage of the porous current collector structure resulting from gas evolution processes, expansion and contraction of the active material during cycling, or other processes (sinter damage). It should be explicitly stated that it is unlikely that these three processes are the sole sources of capacity loss of nickel electrodes in zinc/nickel oxide cells. Indeed, as was mentioned earlier, there is evidence of other phenomena at work, such as drying of the electrodes and the formation of insulating layers within the active material.

Chapter III: Experimental Apparatus and Methods

A variety of physical and chemical methods were employed to characterize the failure of nickel oxide electrodes in zinc-nickel oxide cells. This characterization was accomplished by comparision of failed nickel oxide electrodes with uncycled electrodes and other standard materials. The techniques used in this investigation include x-ray photoelectron spectroscopy (XPS), four-point resistivity measurements, x-ray diffraction of electrode materials, Raman spectroscopy, optical microscopy, and charge-discharge cycling.

Materials studied

Samples were taken from a zinc-nickel oxide cell pack which consisted of three pasted zinc electrodes surrounded by four nickel oxide electrodes. All nickel oxide electrodes studied used porous sintered nickel current collectors and were purchased from Eagle-Picher Industries, Inc. The loading of active material in the nickel electrodes was 1.6 g/cm^3 void space, which is somewhat higher than the 1.3 g/cm^3 void space loading that has been used in other nickel electrodes tested in this laboratory. The cell pack used a reduced-alkalinity electrolyte (3.2 M KOH, 1.8 M KF, 1.8 M K_2CO_3, ZnO saturated), and failed after 200 cycles.

Figure 3.1 displays the capacity / cycle number behavior of this cell pack [49]. The electrode dimensions were 15 cm by 16 cm, with a cell capacity of 21 A-h. It was charged at a C/7 rate, with a constant-voltage limited-current at a cell voltage of 1.95 V. The typical discharge was at a C/3 rate to a cell voltage of 1.0 V, or 80 % depth of discharge (DOD), whichever condition arose first.

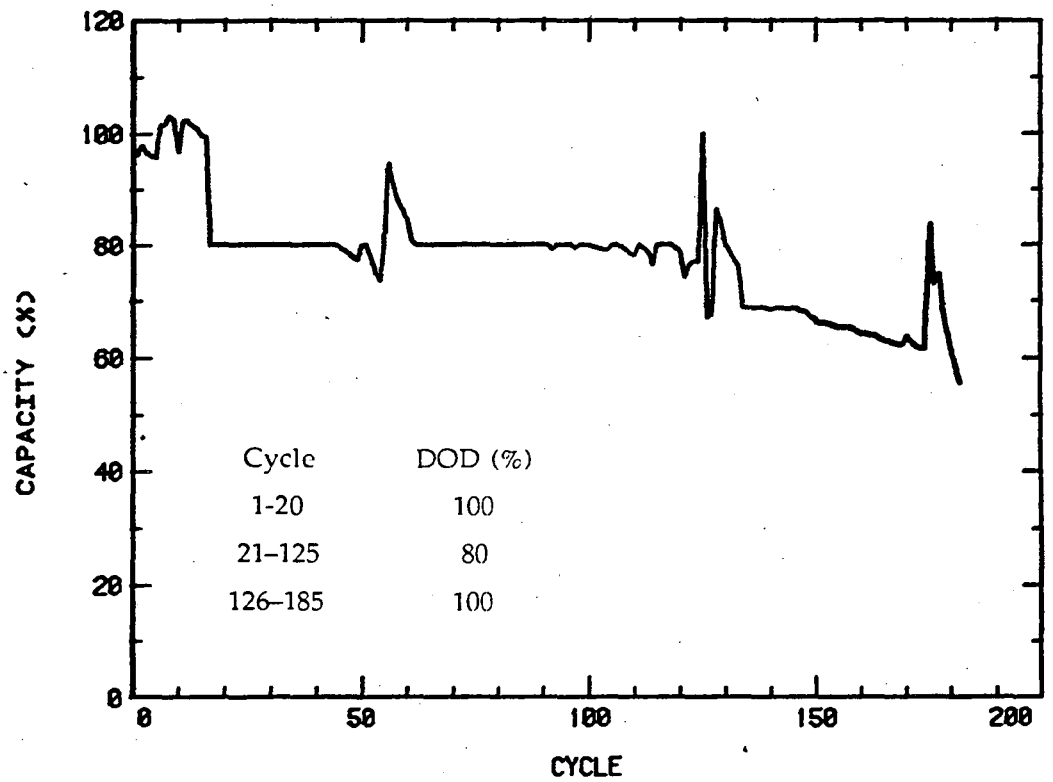

Figure 3.1: Cycling behavior of a 21 A-h zinc-nickel oxide cell utilizing a reduced-alkalinity electrolyte [49].

The spikes at cycles 55, 125, and 175 represent "regeneration" cycles, which consist of a C/10 discharge to a cell voltage of 0 V followed by a C/10 charge, and are intended to help recover some of the lost capacity of the cell. For further details of cell fabrication, consult Adler, et al. [28].

After the cell cycling experiments were completed, the nickel oxide electrodes were removed from the cell, and soaked in water for approximately one week, to remove any excess electrolyte from the pores. The electrodes were then allowed to dry in air at room temperature for an extended period of time (greater than one month), at which time the electrode material was either crushed and chemically analyzed, or was cut into thin strips for resistivity measurements.

Identification of the various phases present in these cycled electrode materials will be accomplished by comparison of their spectra with the spectra of well-defined reference compounds. The commercial sources or methods of synthesis (where applicable) of the reference compounds are listed in Table 3.1. A more-detailed account of the methods of synthesis and characterization by powder x-ray diffraction of these reference compounds is given in the Appendix.

Table 3.1: Preparation or sources of reference compounds

Compound	**Source**
β-$Ni(OH)_2$	Inco, Ltd. (Canada)
β-NiOOH	Glemser [5, 50]
α–$Ni(OH)_2$	Delmas, et. al. [8]
ZnO	Aldrich, 99.999 %
$Zn(OH)_2$	Alfa
α–$(Ni,Zn)(OH)_2$	Bode [6], Romanov [26]

X-ray photoelectron spectroscopy (XPS)

X-ray photoelectron spectroscopy was developed in the 1960s by K. Siegbahn, who received a Nobel Prize for his efforts. The technique is a rather simple one in principle. The general idea is that a sample is irradiated with x-rays of energy $h\nu$, and the kinetic energy of the electrons that are emitted by the photoelectric and Auger effects is measured. The binding energy is defined as follows:

$$\text{Binding Energy} = h\nu - \text{Kinetic Energy}$$

Sources of x-rays in XPS are usually Mg Kα or Al Kα. The energy of the incident x-rays is 1253.6 eV when using a Mg source, and 1486.6 eV when using an Al source. The Mg source is usually preferred, because it has a slightly narrower linewidth.

The two fundamental processes that occur in XPS are photoelectron emission and Auger electron emission. As Figure 3.2 shows, a photoelectron is emitted when a core-level electron is excited by incoming energy (x-rays, in this case). Figure 3.3 shows that emission of Auger electrons occurs by the relaxation of an outer shell electron into a vacant lower energy state, which leads to the (almost) simultaneous emission of an Auger electron. Typically, the spectra are displayed as either counts of emitted electrons versus the (apparent) binding energy of emitted electrons (N(E) vs. E), or counts of emitted electrons normalized by the energy versus binding energy (N(E)/E vs. E) [47]. In this work, the normalized counts versus binding energy convention will be followed.

There are two other features that occur in XPS spectra, so-called "shake-up" peaks, and satellite peaks. Shake-up (or "shake-off") peaks are simply

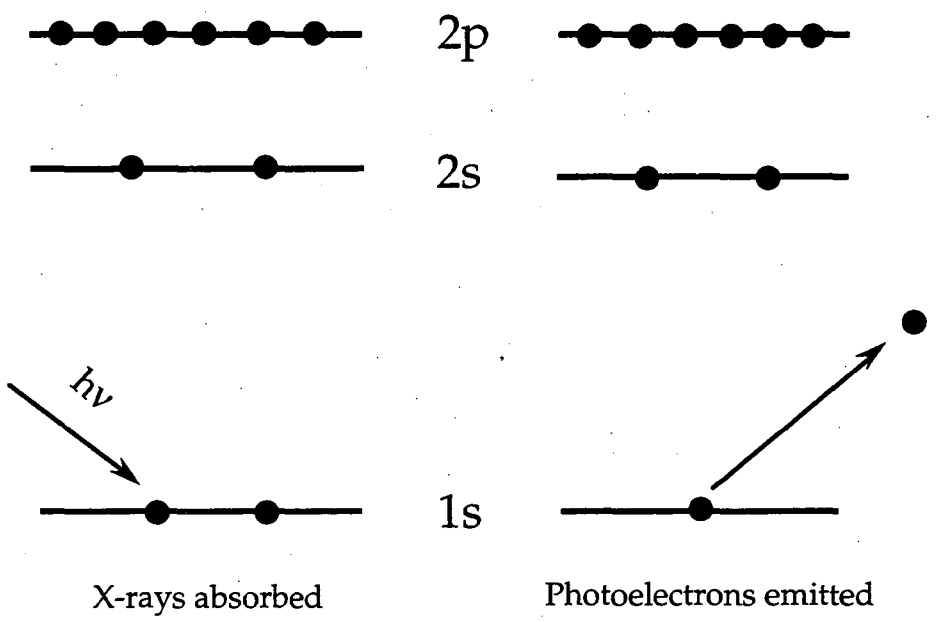

Figure 3.2: Photoelectron emission

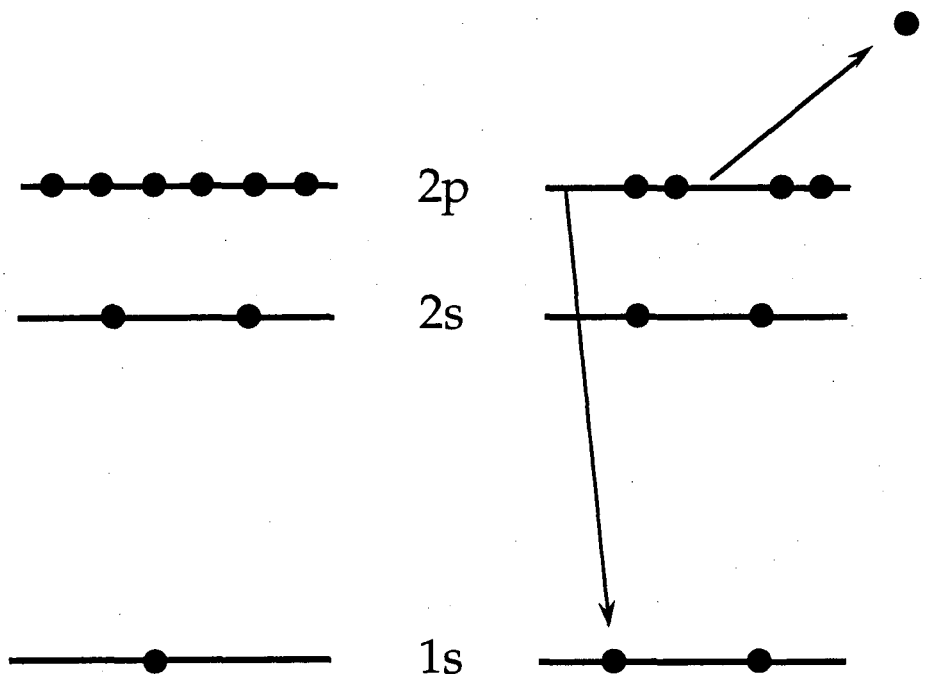

Core-level vacancy created by photoelectron emission

Electron relaxation and and Auger electron emission

Figure 3.3: Auger electron emission

photoelectron emissions from excited states. They usually appear at binding energies several eVs higher than their parent peaks, and are sometimes useful in distinguishing between a metal species (no shake-up peaks present) and a metal oxide (shake-up peaks present). This is the case with nickel, nickel oxide, and nickel hydroxide. Both NiO and $Ni(OH)_2$ exhibit shake-up peaks, whereas Ni metal does not. Because the x-ray energy used is not monochromatic, but appears in several general bands, satellite peaks may appear. For example, the most-intense line of Mg x-rays, the $K\alpha_1$ line, has an energy of about 1253.6 eV, whereas the energy of Mg $K\alpha_2$ line is about 8.4 eV higher with about 8 percent the intensity. Because the x-ray emission spectra of both Mg and Al are well known, their satellite peaks do not present a problem in routine data interpretation [51].

The usefulness of XPS derives from the fact that it is quite surface specific, with an effective depth in most substances of only about 10Å [52]. This feature will allow us to detect passive or pore-blocking materials existing on the surface to the exclusion of the effects of the bulk composition of the sample. Another useful feature of XPS is that it is sensitive to chemical states: that is, chemical shifts are observed (e. g., Zn and ZnO are distinguishable.)

A practical concern is that when using XPS to investigate nonconducting or semiconducting materials, as is the case here, charging of the sample will become a problem [53]. Some method of either eliminating or at least accounting for this charging must be found. Pressing the powdered samples into indium foil was initially attempted to reduce charging of the various nickel samples. Using vacuum-deposited gold as a reference was also attempted. Ultimately, it was found that the best procedure was to mount all powdered samples on double-sided adhesive tape, and to use the adventitious carbon photoelectron peak, C 1s, as a reference, assigning it a binding energy

value of 284.6 eV. This was the simplest method of mounting the samples, and yielded the best results.

The XPS unit was a Perkin-Elmer PHI 5300 unit. In all cases, unless otherwise noted, a Mg x-ray source was used, at a power setting of 500 W, and a 15 kV potential applied to the anode. All spectra were referenced to the adventitious carbon line and in all cases the pressure inside the UHV chamber was 4.0×10^{-8} torr or lower.

Raman Spectroscopy

A few Raman spectra were acquired by D. Littlejohn of LBL in an attempt to find structural differences between α–$Ni(OH)_2$ and α–$(Ni, Zn)(OH)_2$. The region from 280 cm^{-1} to 510 cm^{-1} was scanned to observe lattice vibrational modes, if present. The excitation source was a Coherent 90-5 argon-ion laser (514.5 nm, 50 mW). The Raman-scattered light was passed through a Spex 1403 double monochromator and was detected with a thermoelectric-cooled RCA 31034 photomultiplier tube. The apparatus was controlled with a Spex Datamate data acquisition system.

Resistivity measurements

As mentioned earlier, Fritts [19, 20] observed a general resistivity increase of nickel oxide electrodes on extended cycling in cadmium/nickel oxide cells. His studies, however, were of an averaging type, measuring the increase within an entire electrode. It is useful to determine if such a resistivity increase occurs in electrodes cycled in a reduced-alkalinity electrolyte. In addition, it is appropriate to measure the spatial dependence of an observed resistivity increase.

The measurements made here were of the four-point (Kelvin) probe type, to reduce any errors due to contact resistance. The current source was a Princeton Applied Research PAR 273 potentiostat / galvanostat, operating in galvanostatic mode. The potential drop was measured with a Keithley Model 616 digital electrometer. Samples of cycled electrode material were sectioned into pieces measuring 4 cm by 0.35 cm. A low-speed wafering saw (Buehler) with a high-concentration diamond blade (Buehler) was used to minimize cutting damage to the electrode material. Several different mounting arrangements were tried, but the one shown in Figure 3.4 was simplest. It used aluminum foil strips glued to a piece of acrylic to provide a fixed and reproducible measurement.

Figure 3.5 displays possible configurations of leads for the resistivity measurement. All measurements made in this work were done as indicated in Figure 3.5 (a); that is, with all leads on the same side of the electrode. There had been some concern that lead placement might affect the measured values of resistivities. Alternate placements were tried, such as Figure 3.5 (b). It was found that the maximum variation with placement configuration was only about ± 2.5 percent.

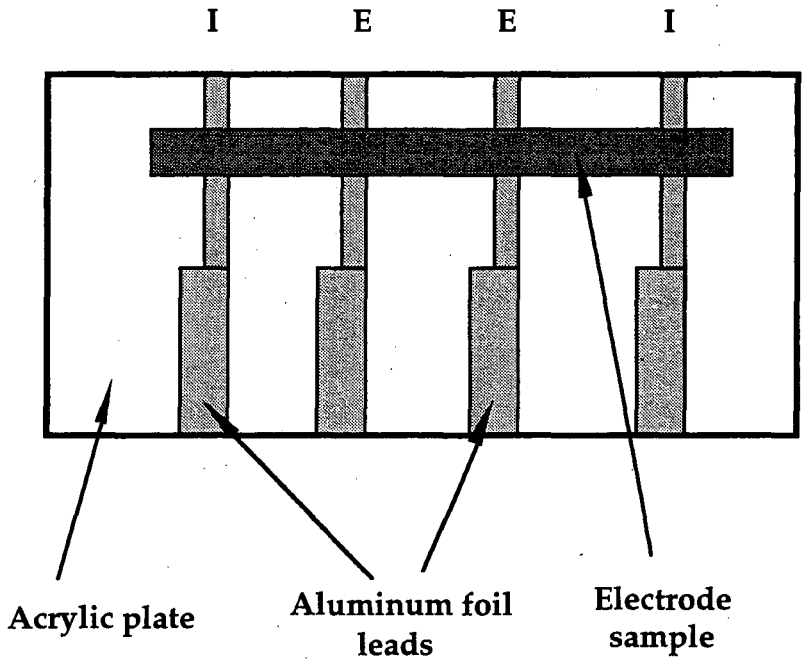

Figure 3.4: Four-point probe method for resistivity measurements.

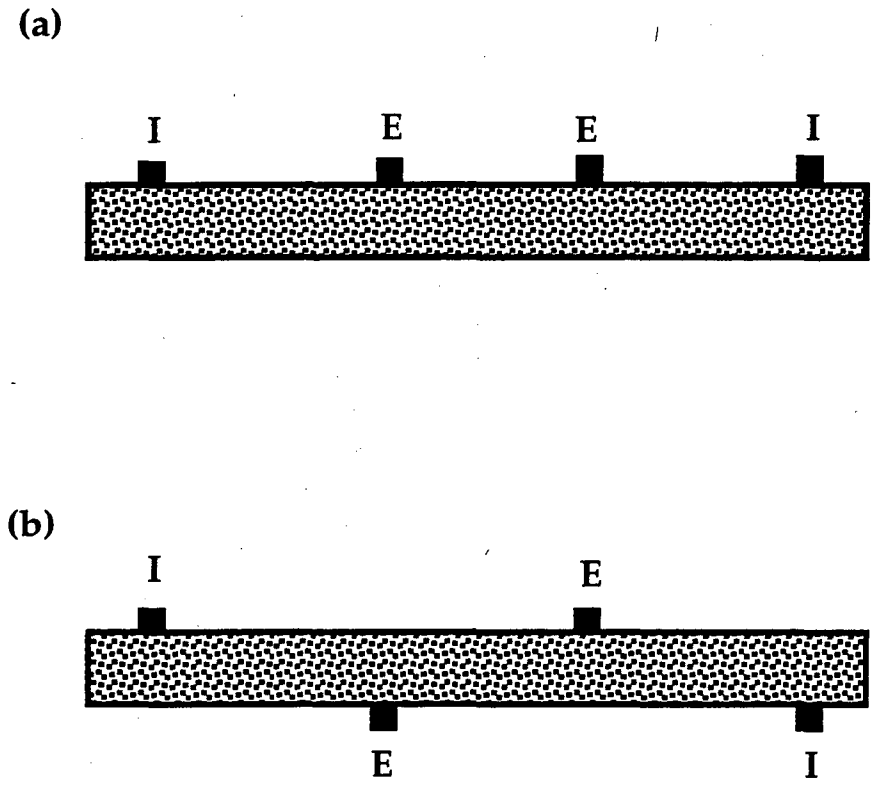

Figure 3.5: Positioning of leads for four-point resistivity measurements.

(a): Configuration used. (b) Alternate configuration tested.

Galvanostatic charge / discharge studies

Important information would be gained if one could distinguish between passivation or pore-blockage of the surface, and mechanical degradation of the sintered nickel electrode structure. Certainly, the presence or absence of pore-blocking species or of a resistivity increase would be noteworthy, but further information would be needed to distinguish in a qualitative manner the relative importance of the two.

Initially, consideration was given to an attempt to define the amount of active-material isolation by simply charging a completely discharged nickel oxide electrode, and then using an "active oxygen" test [e. g. 5] to determine the final oxidation state of the active material. By knowing the number of coulombs of charge introduced into the system, and knowing the final average oxidation state of the system, one could quantify the amount of active material rendered inactive by various degradation processes. This approach, however, still does not clarify the question of the relative importance of the processes of passivation or pore blockage of the electrode surface, and mechanical damage of the sintered nickel structure in the capacity loss of the nickel oxide anodes. Therefore, another approach was used.

The galvanostatic charge / discharge experiments carried out here were of the standard three-electrode arrangement (Figure 3.6). The working electrode was of the same cycled electrode material as was used in the resistivity measurements. The counter electrode was constructed of initially uncycled material, subjected to five formation cycles in a 5.9 M KOH (45 w/o KOH aqueous solution, J. T. Baker, "Baker Analyzed" grade) and 1.1 M LiOH (EM Science, reagent grade). Water was obtained from a Millipore high-resistivity water purification system (ρ = 15 MΩ-cm or greater). The superficial dimensions of both electrodes were 9.5 mm by

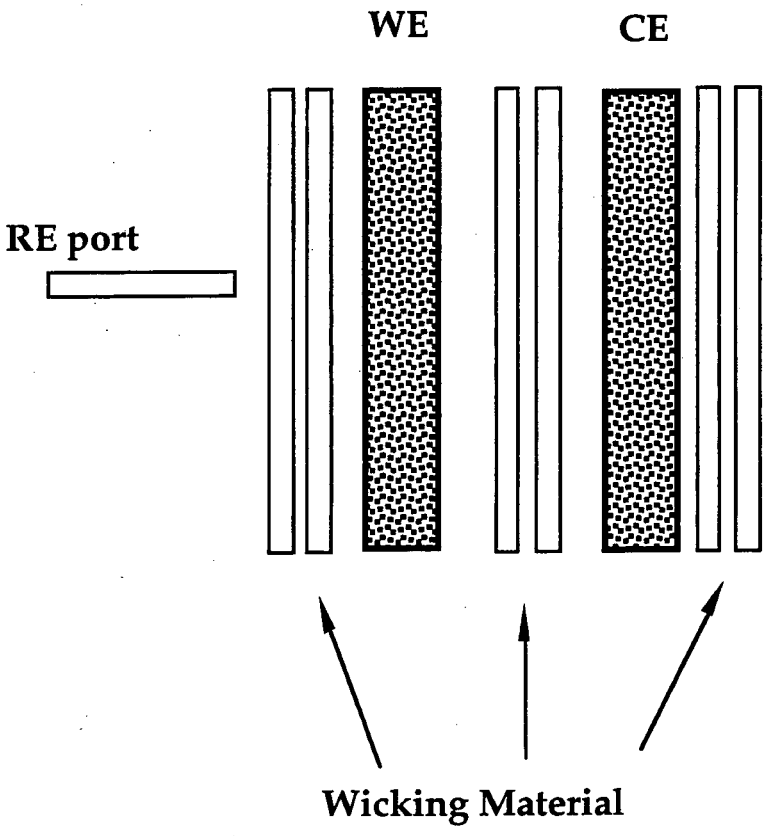

Figure 3.6: Schematic of cell used in most cycling experiments.

10.5 mm. The capacity of this electrode was 31.9 mA-h. A Hg/HgO reference electrode was used. Pellon 2524 nonwoven nylon wicking material (Freudenberg Nonwoven, Chelmsford, Massachusetts) provided wetting and mechanical separation of the electrodes. The electrolyte used in all cycling experiments was 5.9 M KOH, 1.1 M LiOH, with an excess of ZnO (EM Science, reagent grade) added to achieve saturation. A small amount (370 mg/L or 1100 mg/L) of the surfactant Triton X-100 (Spectrum Chemical, Gardenas, CA) was added in most instances.

A simple charge-discharge scheme was chosen. First, the electrode was charged at a C/6 rate, with a constant-voltage tapering begun at a potential of 530 mV vs. Hg/HgO, for a total charging time of six hours. A 15 minute open-circuit period between charge and discharge was used. The cell was then discharged at a C/6 rate (equivalent to a current density of 5.33 mA/cm^2) until the working electrode reached a potential of 0 mV vs. Hg/HgO. In some cases, the cell was charged and discharged more slowly (C/15 rate, or a current density of 2.13 mA/cm^2) to assess the rate dependence of the process.

The goals of these measurements were quite simple. Initially, several cycles of the electrode were made in a surfactant-free electrolyte to measure a relatively stable baseline capacity. Then, various modifying treatments were applied in series. To test the idea that a loss of wetting may cause a capacity loss in nickel electrodes, the electrodes were operated in an electrolyte containing Triton X-100. No attempt was made to find either an optimal wetting agent for the system, or an optimal concentration of surfactant. The intent was merely to see if a commonly available wetting agent would influence the measured discharge capacity of the electrode. After this experiment, the nickel electrode was washed in a 20 w/o KOH solution (J.T. Baker, "Baker Analyzed") to remove any zinc species which could

presumably contribute to a capacity loss. The first washing was at 20° C for 18 hours. Fresh KOH solution was used for a second washing at 60° C for 18 hours. Finally, the electrodes were cycled under various degrees of compression (see Figure 3.7), to determine if one could influence the (presumed) loss of physical contact between active material and current collector. The specifics of these modifying conditions are listed in Table 3.2.

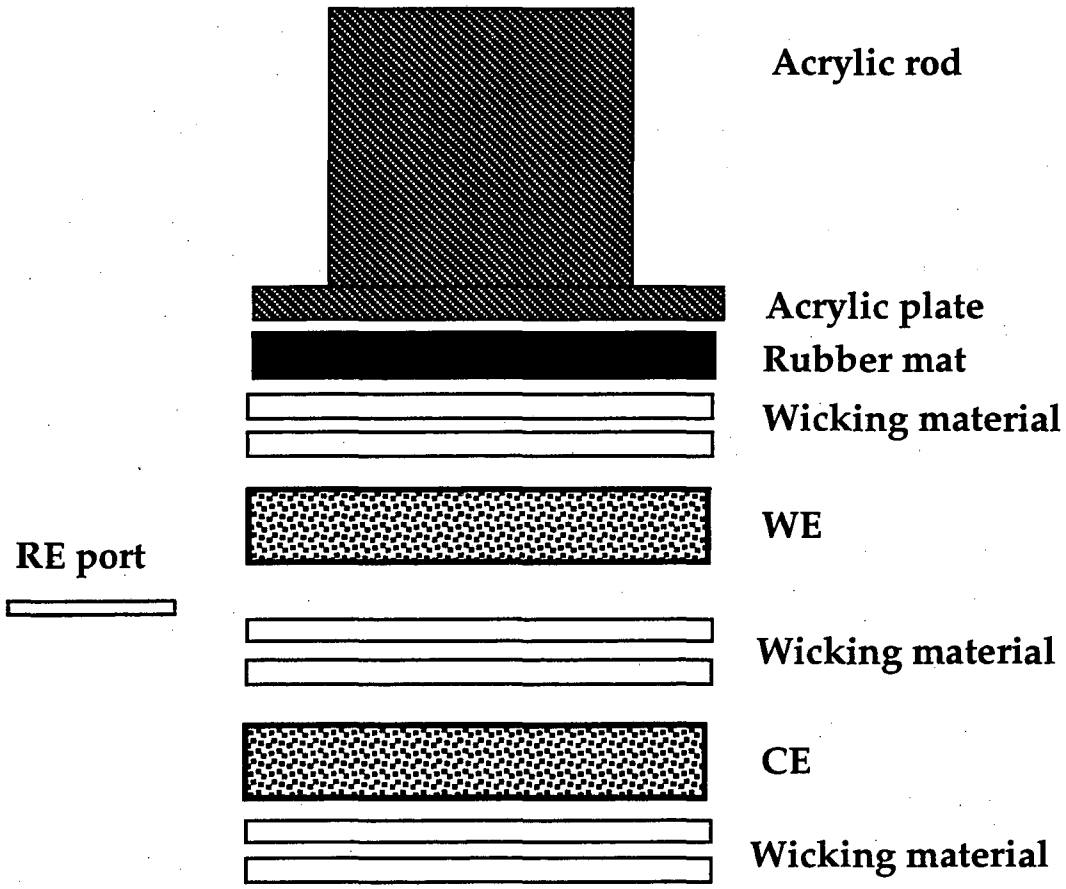

Figure 3.7: Schematic of cell used in cycling with compression.

Table 3.2: Summary of cycling experiments

Run	Modifying Treatment	Triton X-100 Concentration	Effect Examined
A	None	None	Establish baseline
B	Surfactant	370 mg/L	Wetting
C	Surfactant	1100 mg/L	Wetting
D	Washing: 20 w/o KOH, room temp., 18 hours followed by washing at 60 deg. C for one day.	370 mg/L	Pore blockage or nickel hydroxy-zincate formation
E	Compression, 310 kN / m^2	370 mg/L	Reversibility of sinter damage
F	Compression, 675 kN / m^2	370 mg/L	Reversibility of sinter damage
G	Compression, 2070 kN / m^2	370 mg/L	Reversibility of sinter damage

Note: All cycles were run with 5.9 M KOH, 1.1 M LiOH, and ZnO saturated. All cycles run at a C/6 charge (taper at 530 mV) and C/6 discharge, except for run D, which was run at C/15 charge and C/15 discharge.

Chapter IV: Results and Discussion

The experimental techniques used in this work include XPS, four-point resistivity measurements, galvanostatic charge and discharge experiments, and other supplementary methods. We begin first by examining the results of the XPS study.

X-ray photoelectron spectroscopy (XPS)

It is helpful to examine some of the general features of photoelectron spectra of model compounds of interest before beginning a closer examination of all results. Figure 4.1 is a photoelectron survey spectrum of β-$Ni(OH)_2$, and Figure 4.2 is a survey spectrum of ZnO. Tables 4.1 and 4.2 identify the peaks shown in Figures 4.1 and 4.2 respectively. Among the features of note are the rather complex Auger structures of O, Ni, and Zn. One should also recognize that nickel hydroxides also exhibit the shake-off peaks mentioned earlier. The adventitious C peak, which is used for charge referencing here, is quite weak. In Figure 4.3, we compare the Zn $2p_{1/2}$ spectra of ZnO and $Zn(OH)_2$. As one can note, there is a small binding energy shift, but little other difference in the Zn $2p_{1/2}$ spectra. The Zn $2p_{1/2}$ binding energy for ZnO of 1020.8 eV is somewhat lower than a published value of 1021.9 eV [53]. The binding energy of $Zn(OH)_2$ was measured to be 1021.5 eV.

We now turn to the spectra of the various nickel oxides of interest. Figure 4.4 displays the Ni 2p doublet. Note the shake-off peaks at about 862 eV and 878 eV. The Ni 2p spectra of phases involved in nickel electrode cycling, β–$Ni(OH)_2$ and β–NiOOH, are shown in Figure 4.5. Both phases exhibit the same general shape, with β–NiOOH having a slightly

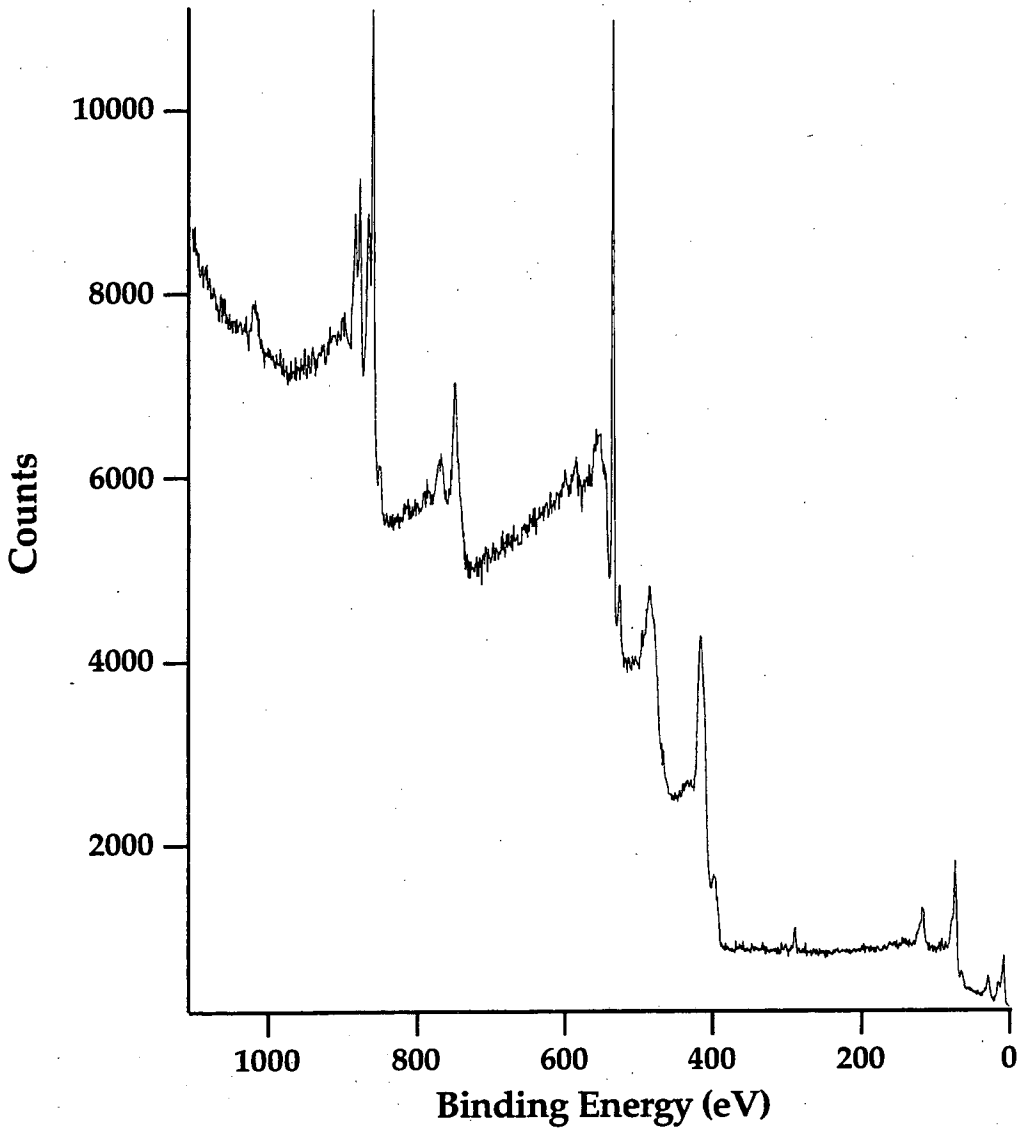

Figure 4.1: Survey photoelectron spectrum of β-$Ni(OH)_2$

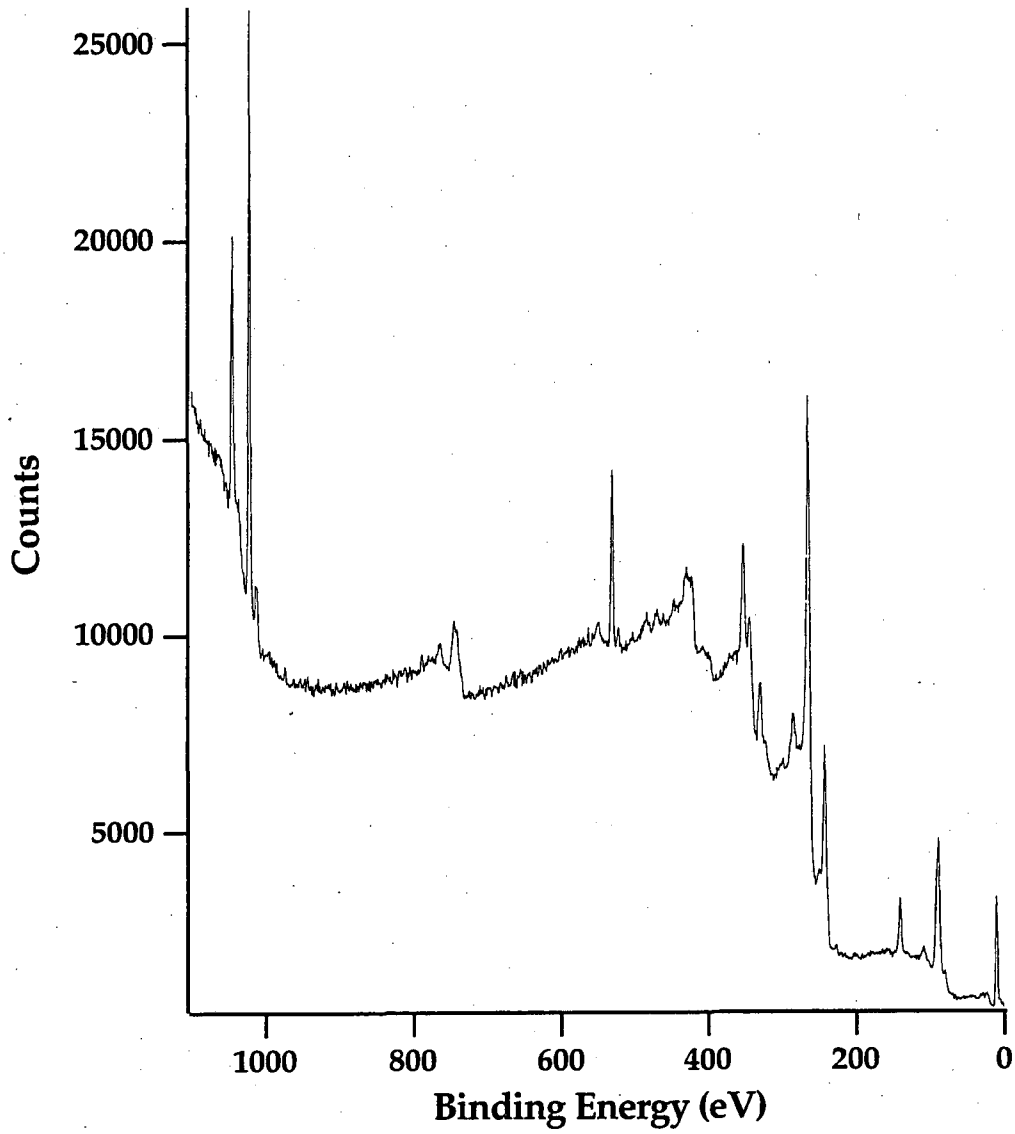

Figure 4.2: Survey photoelectron spectrum of ZnO

Table 4.1: Peak identification for β-$Ni(OH)_2$ survey spectrum

Binding Energy (eV)	Peak Identification	Comments
1020	C KLL Auger	Weak
890-850	Ni $2p_{1/2}$, $2p_{3/2}$ doublet	Strong, shake-off peaks
790-740	O KVV Auger	
610-540	Ni LMM Auger	
535	O 1s	Strong
490-420	Ni LMM Auger	Strong, broad
285	C 1s	Weak
120	Ni 3s	
74	Ni 3p	
30	O 2s	

Table 4.2: Peak identification for ZnO survey spectrum

Binding Energy (eV)	Peak Identification	Comments
1045, 1022	Zn $2p_{1/2}$, $2p_{3/2}$ doublet	Sharp, strong
790-740	O KVV Auger	Broad, weak
530	O 1s	Sharp, strong
430-325	Zn LMM Auger	
285	C 1s	Weak
270-245	Zn LMM Auger	
142	Zn 3s	
90	Zn 3p	
12	Zn 3d	

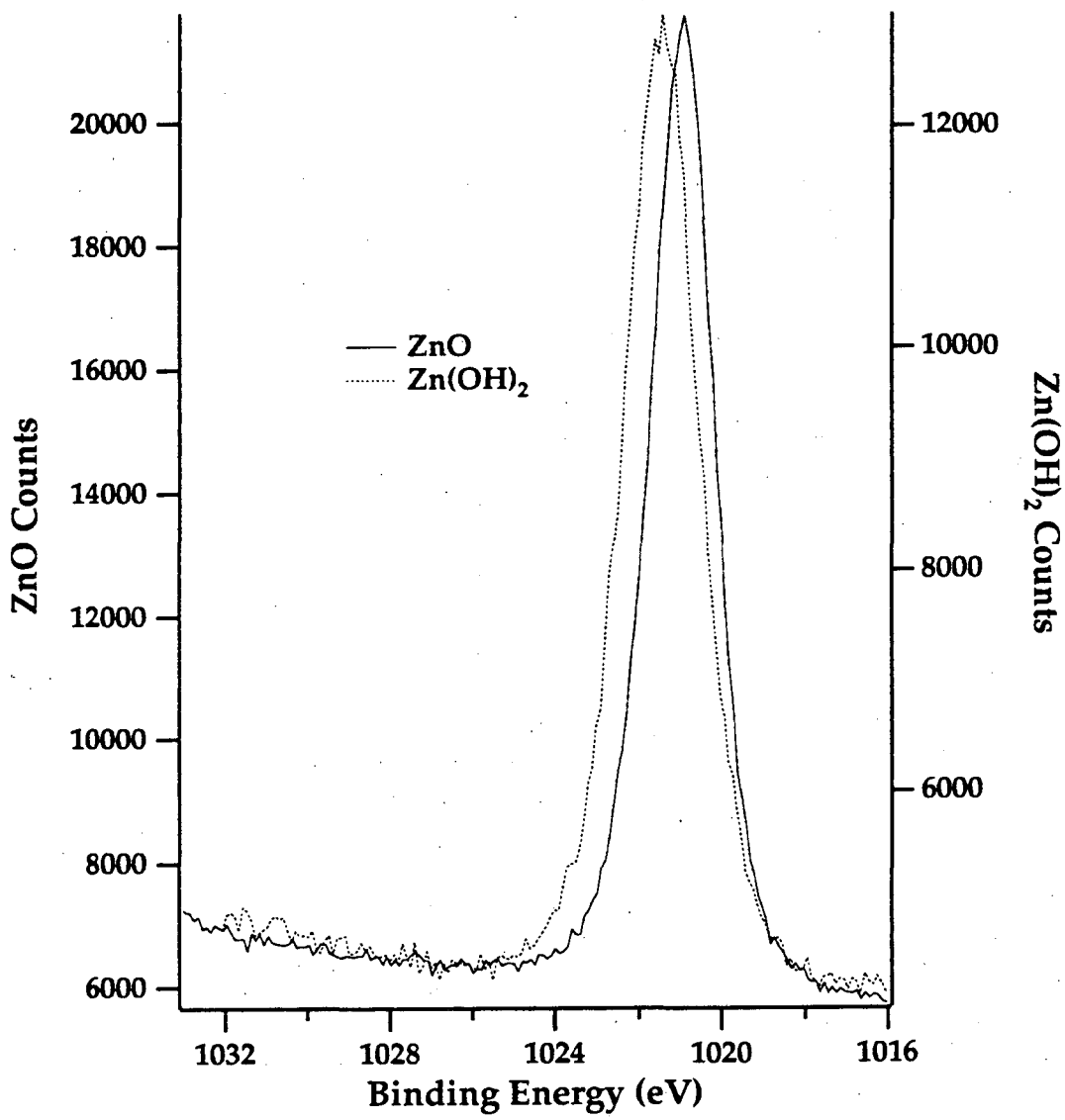

Figure 4.3: Zn $2p_{1/2}$ photoelectron spectra of ZnO and $Zn(OH)_2$

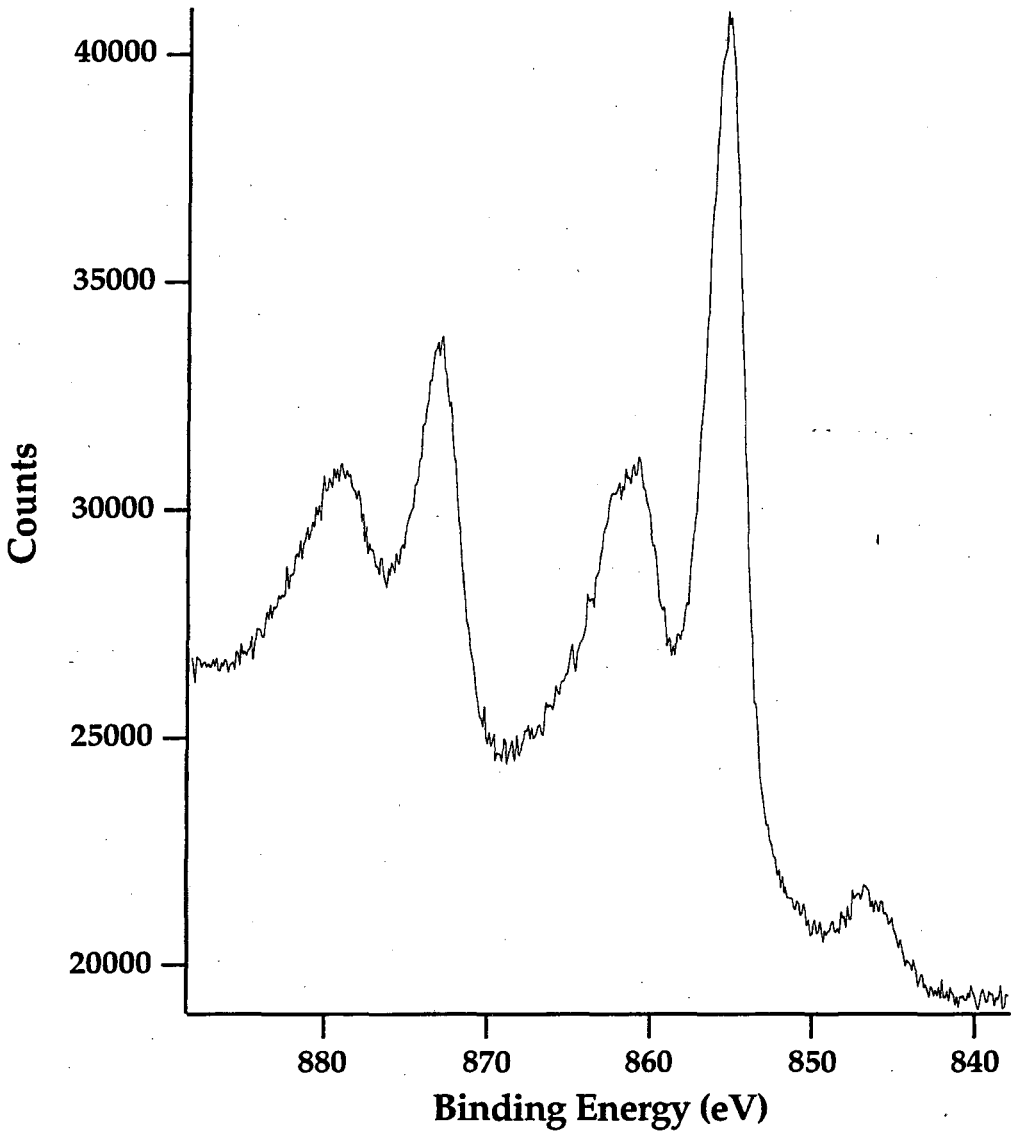

Figure 4.4: Ni $2p_{3/2}$ / $2p_{1/2}$ photoelectron spectrum of β–$Ni(OH)_2$.

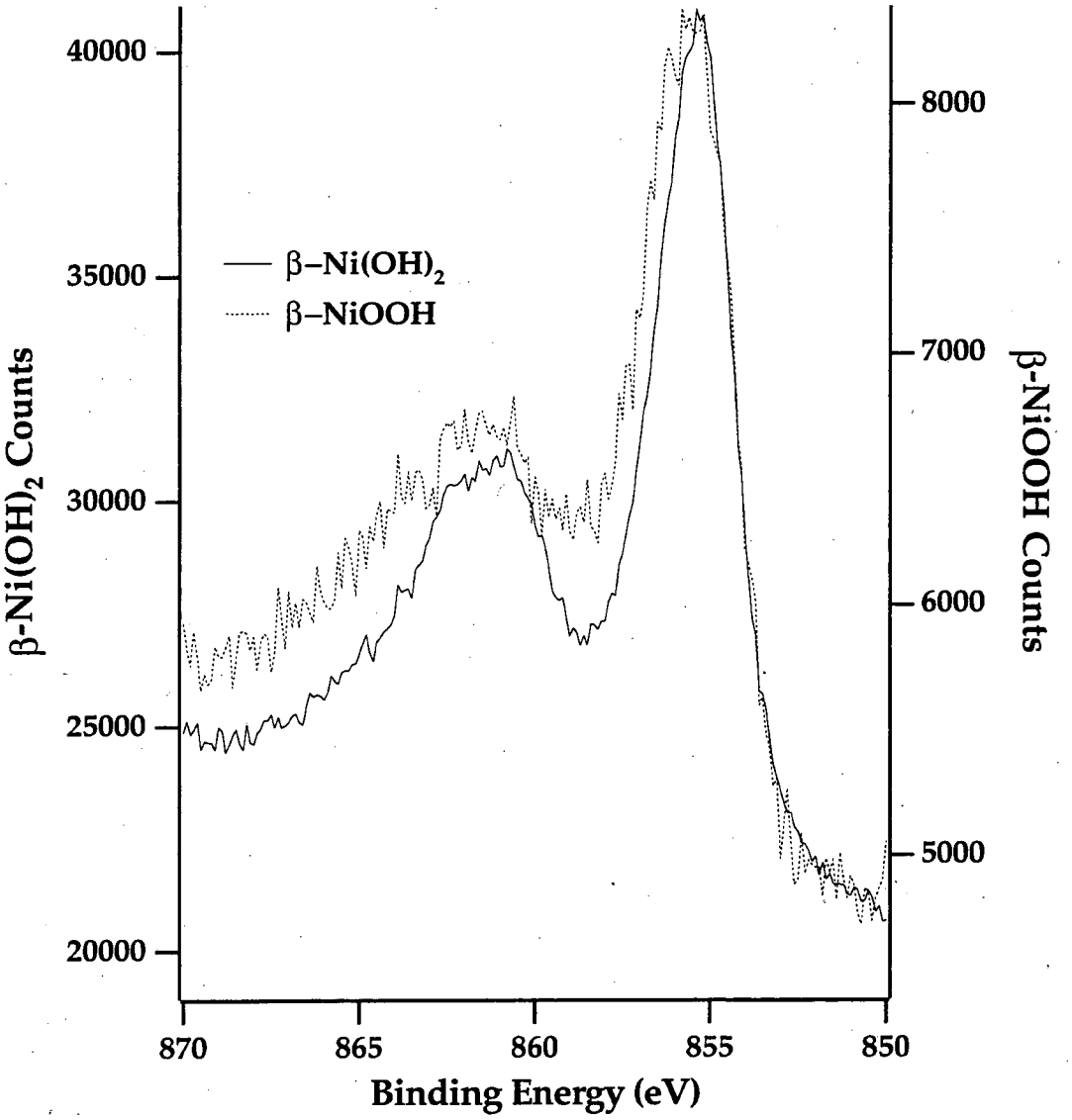

Figure 4.5: Ni $2p_{3/2}$ photoelectron spectra of β–$Ni(OH)_2$ and β–NiOOH.

higher peak binding energy of 855.6 eV versus the 855.3 eV of β–$Ni(OH)_2$. The Ni $2p_{3/2}$ spectra of α–$Ni(OH)_2$ and β–$Ni(OH)_2$ in Figure 4.6 reveal that there is little if any observable difference in binding energies in this case.

As mentioned earlier, there has been speculation that a nickel hydroxyzincate may be responsible for some capacity loss in nickel electrodes when used in nickel-zinc cells. Two nickel hydroxyzincates were prepared, one with a Ni : Zn ratio of 1 : 1 and the other with a Ni : Zn ratio of 10 : 1. Figure 4.7 compares the Zn $2p_{3/2}$ spectra of a nickel hydroxyzincate with a Ni : Zn ratio equal to 10 : 1 and $Zn(OH)_2$. As one can see, there is little peak binding energy difference between these two materials. Figure 4.8 shows that there is little binding energy difference between the Zn $2p_{3/2}$ spectra of the nickel hydroxyzincate with a Ni : Zn ratio of 1 : 1 and $Zn(OH)_2$. The Ni $2p_{3/2}$ spectra of the 10 : 1 nickel hydroxyzincate and that of α–$Ni(OH)_2$ are compared in Figure 4.9. The peak shapes and positions are almost identical. The Ni $2p_{3/2}$ peak position of the 10 : 1 nickel hydroxyzincate is about 0.3 eV greater than that of the 1 : 1 Ni : Zn ratio material.

In an attempt to clarify this ambiguity concerning the nature of the nickel hydroxyzincates, Raman spectroscopy was used. Figure 4.10 displays the Raman spectra of α–$Ni(OH)_2$ and 1:1 α–$(Ni,Zn)(OH)_2$. The region scanned is characteristic of lattice vibrational modes of both nickel and zinc hydroxides. Presumably, if zinc is substituted for nickel to form a "true" nickel hydroxyzincate compound, the Ni-O lattice mode would be altered to some extent. As the figure shows, only the Ni-O vibrational mode is present [e.g. 54], with both the peak position and full-width at half-maximum being the same in both spectra. No band characteristic of a

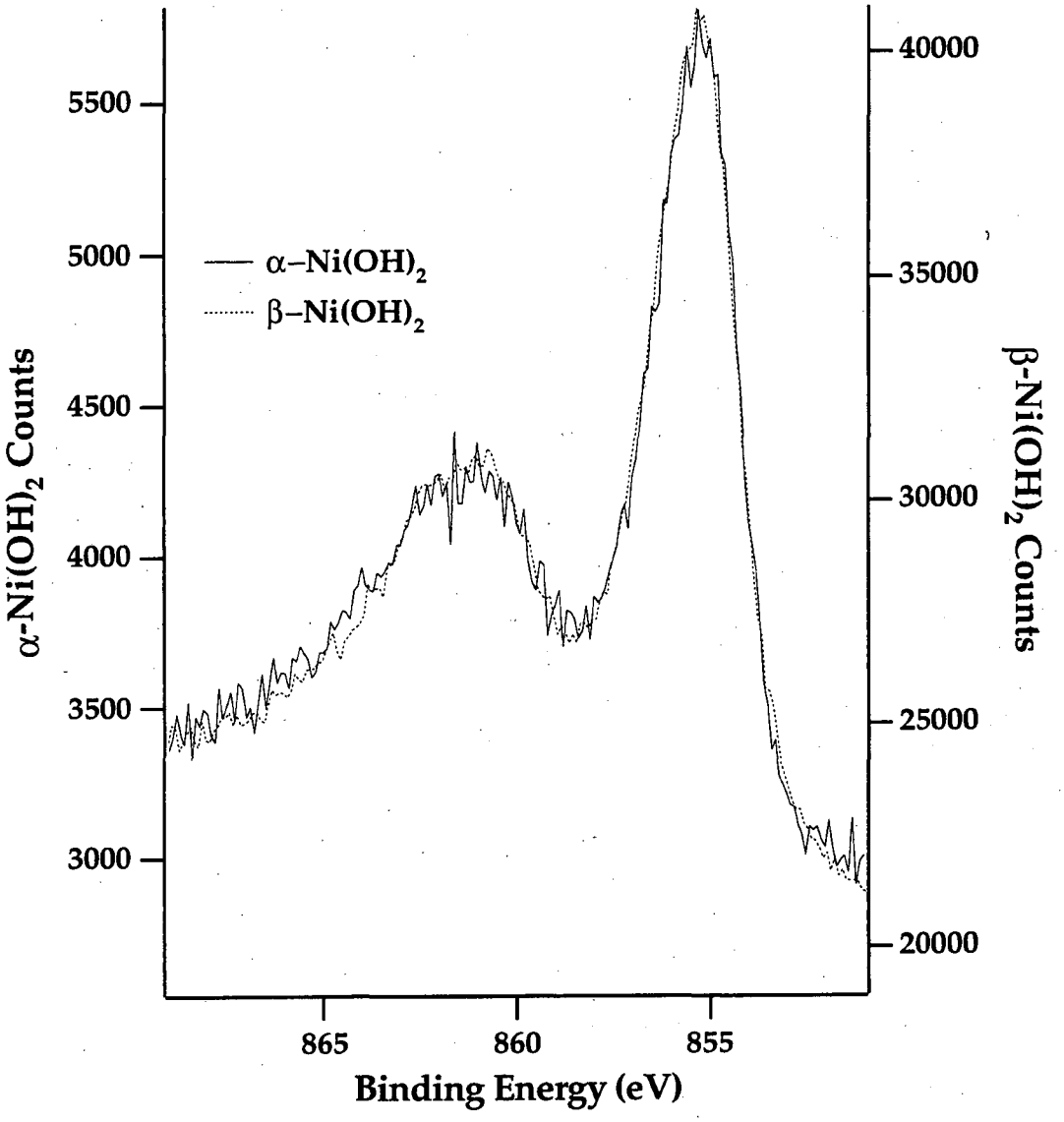

Figure 4.6: Ni $2p_{3/2}$ photoelectron spectra of α–$Ni(OH)_2$ and β–$Ni(OH)_2$.

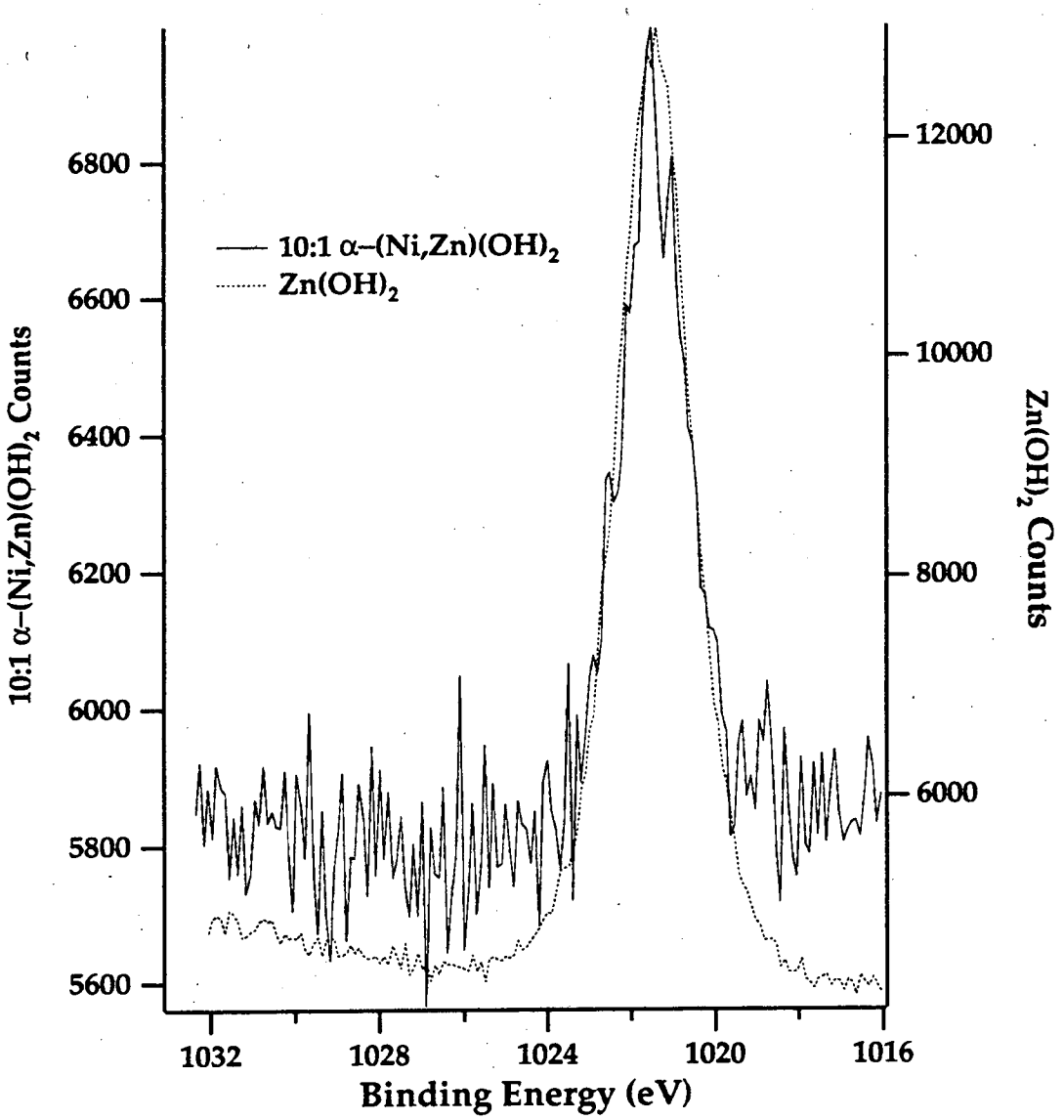

Figure 4.7: Zn $2p_{3/2}$ photoelectron spectra of α–(Ni,Zn)$(OH)_2$ and $Zn(OH)_2$ (Ni : Zn ratio = 10 : 1).

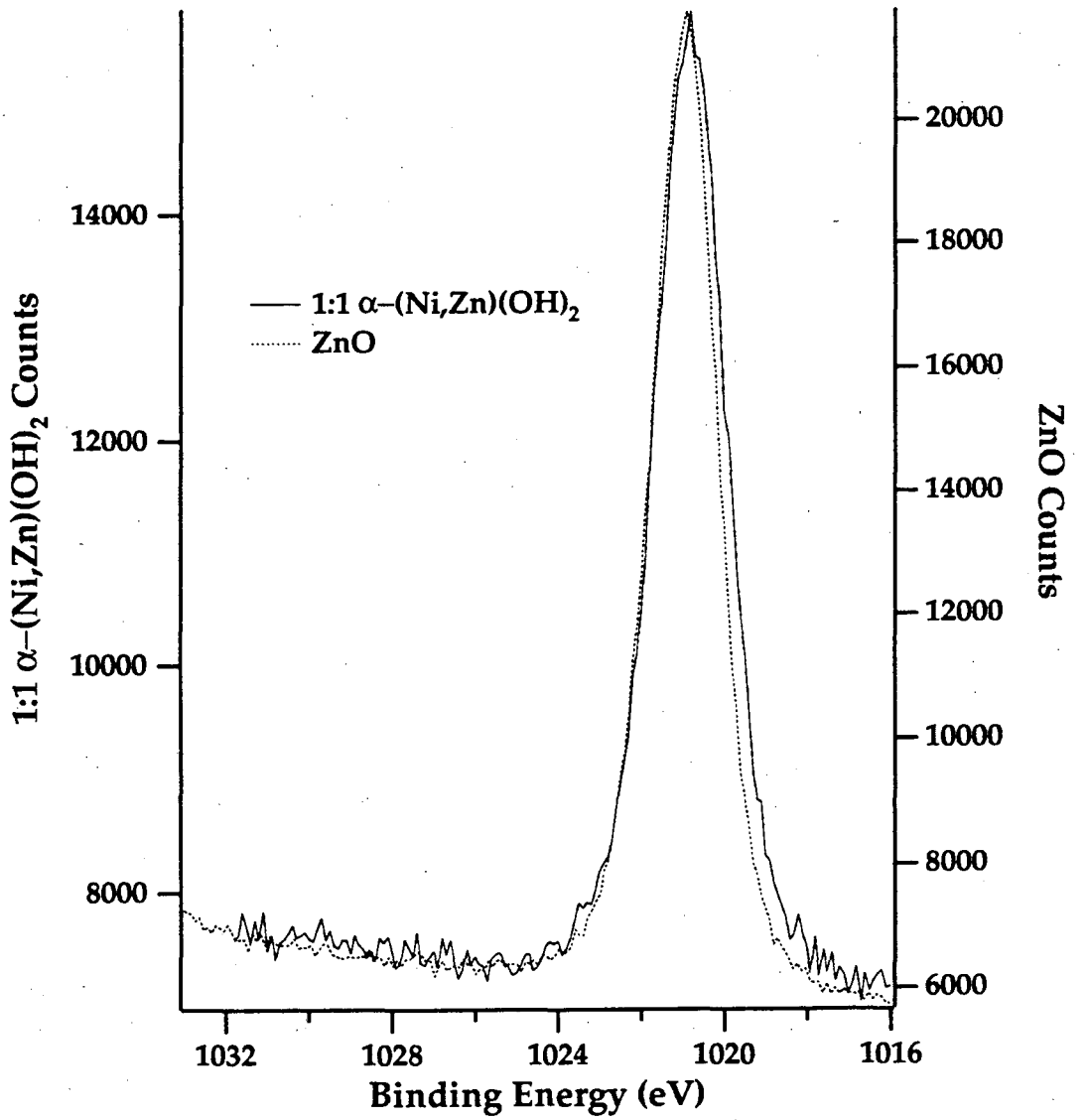

Figure 4.8: Zn $2p_{3/2}$ photoelectron spectra of α–(Ni,Zn)$(OH)_2$ and ZnO (Ni : Zn ratio = 1 : 1).

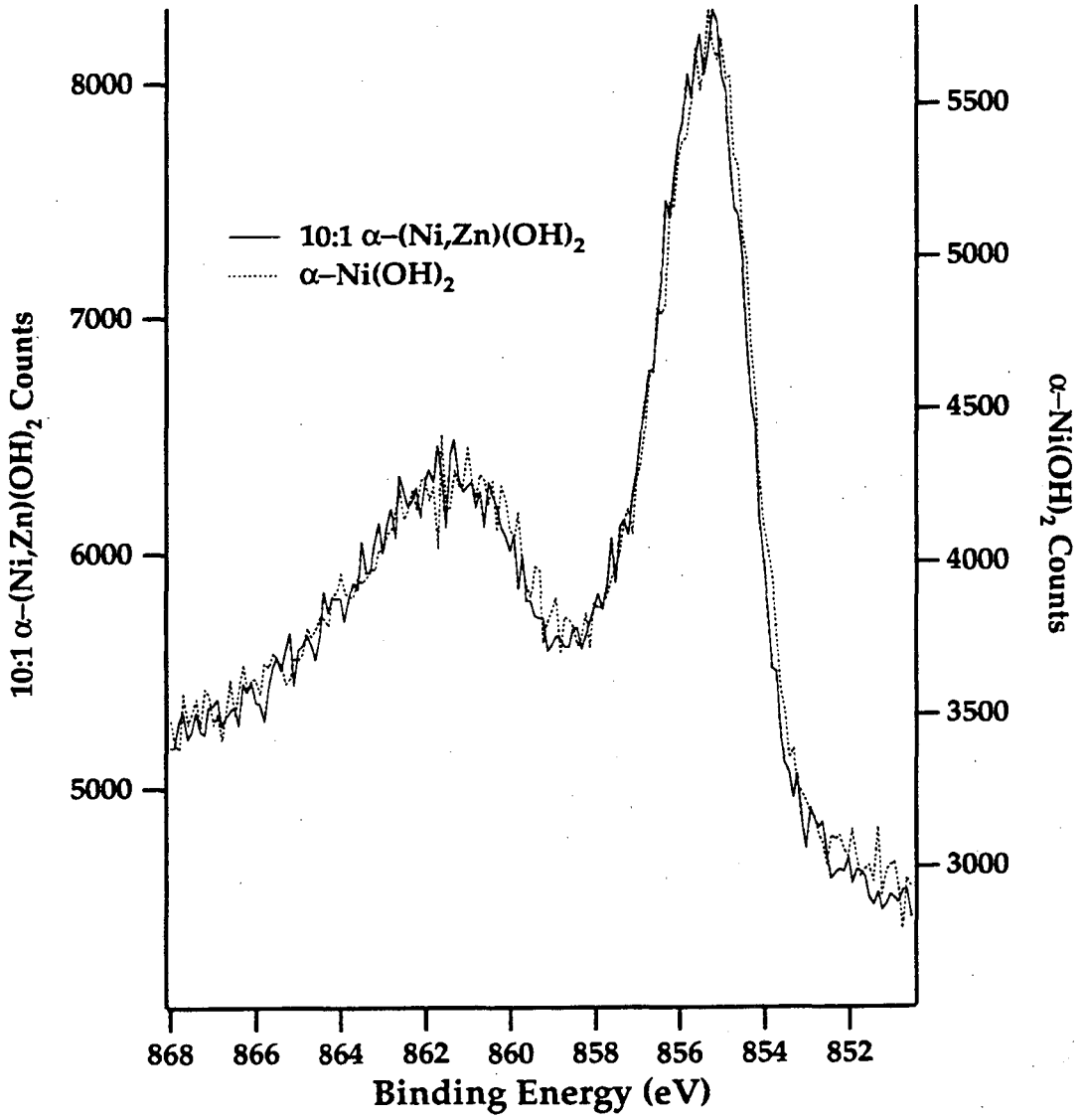

Figure 4.9: Ni $2p_{3/2}$ photoelectron spectra of α–(Ni,Zn)$(OH)_2$ (Ni : Zn ratio = 10 : 1) and α–Ni$(OH)_2$.

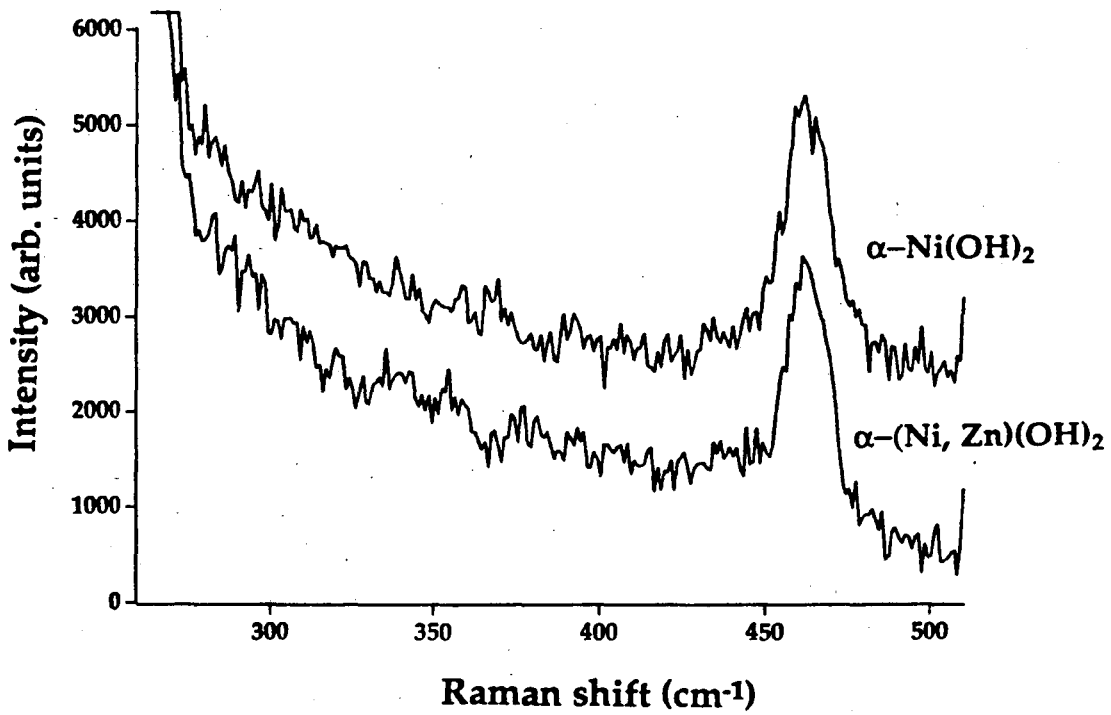

Figure 4.10: Raman spectra of α–$Ni(OH)_2$ and 1:1 α–$(Ni,Zn)(OH)_2$

Zn-O vibrational mode is present, although some forms of $Zn(OH)_2$ are known to lack Raman activity in this region [55]. In short, Raman spectroscopy gives no evidence that Zn can be substituted into the Ni-O lattice, suggesting that the nickel hydroxyzincate is probably a co-precipitate of α–$Ni(OH)_2$, and a form of $Zn(OH)_2$ lacking the structural order to render it Raman active.

Further work needs to be done in characterizing these nickel hydroxyzincates. Bode et. al [6] state that these compounds will exhibit x-ray diffraction patterns similar to that of α–$Ni(OH)_2$, which was confirmed here (see Appendix for XRD patterns). Since none of these compounds exhibit long-range order, however, a better method of structural characterization, such as EXAFS, may have to be employed.

Comparison of cycled and uncycled materials

The most immediate question in this work is whether the use of a reduced-alkalinity electrolyte for the standard KOH/LiOH electrolyte in a zinc-nickel oxide cell will induce observable chemical or structural changes in the nickel electrode, such as the formation of nickel hydroxyzincates, or of water-insoluble fluoride or carbonate species. These could presumably passivate or physically block the electroactive surface of the electrode, resulting in capacity loss. Figure 4.11 compares the Ni $2p_{3/2}$ spectra of electrode material cycled in the reduced-alkalinity electrolyte with β–$Ni(OH)_2$. One observes a slight binding energy difference of less than 0.2 eV. The Zn $2p_{3/2}$ spectra of electrode material cycled in the reduced-alkalinity electrolyte and $Zn(OH)_2$ are compared in Figure 4.12. The peak binding energies agree well. The Ni $2p_{3/2}$ spectra and Zn $2p_{3/2}$ spectra of electrode materials cycled in standard electrolytes and in reduced-alkalinity electrolytes are compared in Figures 4.13 and 4.14. Here we find good agreement in the peak binding energies.

There was no fluoride detected by XPS in any of the cycled electrode samples, which would tend to rule out the possibility of a nickel fluoride or zinc fluoride compound blocking the pores of the nickel electrode. It appears that by using XPS, one cannot observe much difference between nickel electrode materials cycled in standard electrolyte and materials cycled in a reduced-alkalinity electrolyte.

The stability of zinc species in alkaline environments was also examined. An attempt was madeto remove the Zn from nickel hydroxyzincate (Ni / Zn = 1) by washing it in hot 45 w/o KOH (J. T. Baker) at 90° C for 3 hours. The result is shown in Figure 4.15. All Zn is clearly removed, within the detection limits of the technique. The same process

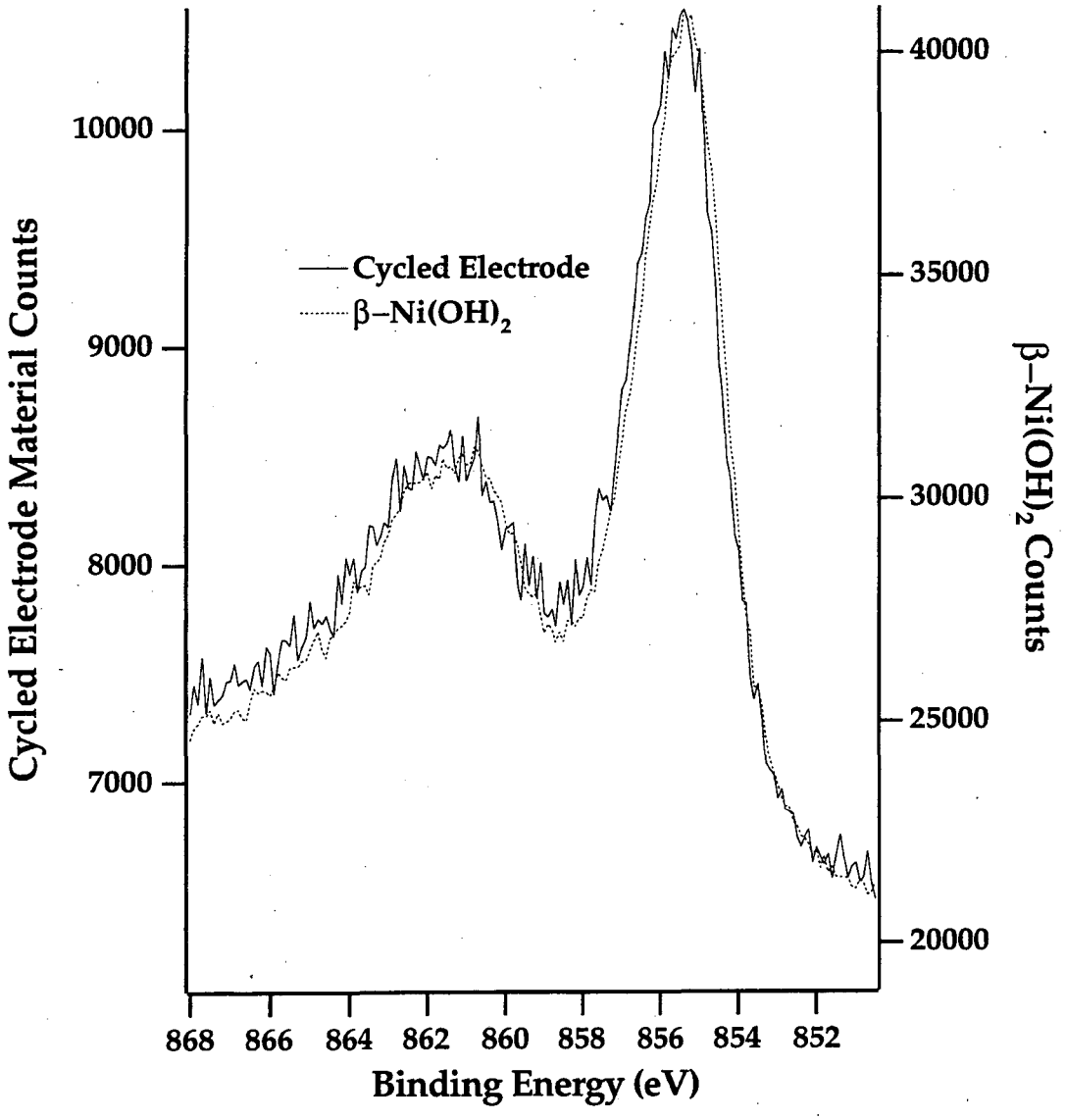

Figure 4.11: Ni $2p_{3/2}$ spectra of nickel electrode material cycled in reduced alkalinity electrolyte and β–$Ni(OH)_2$

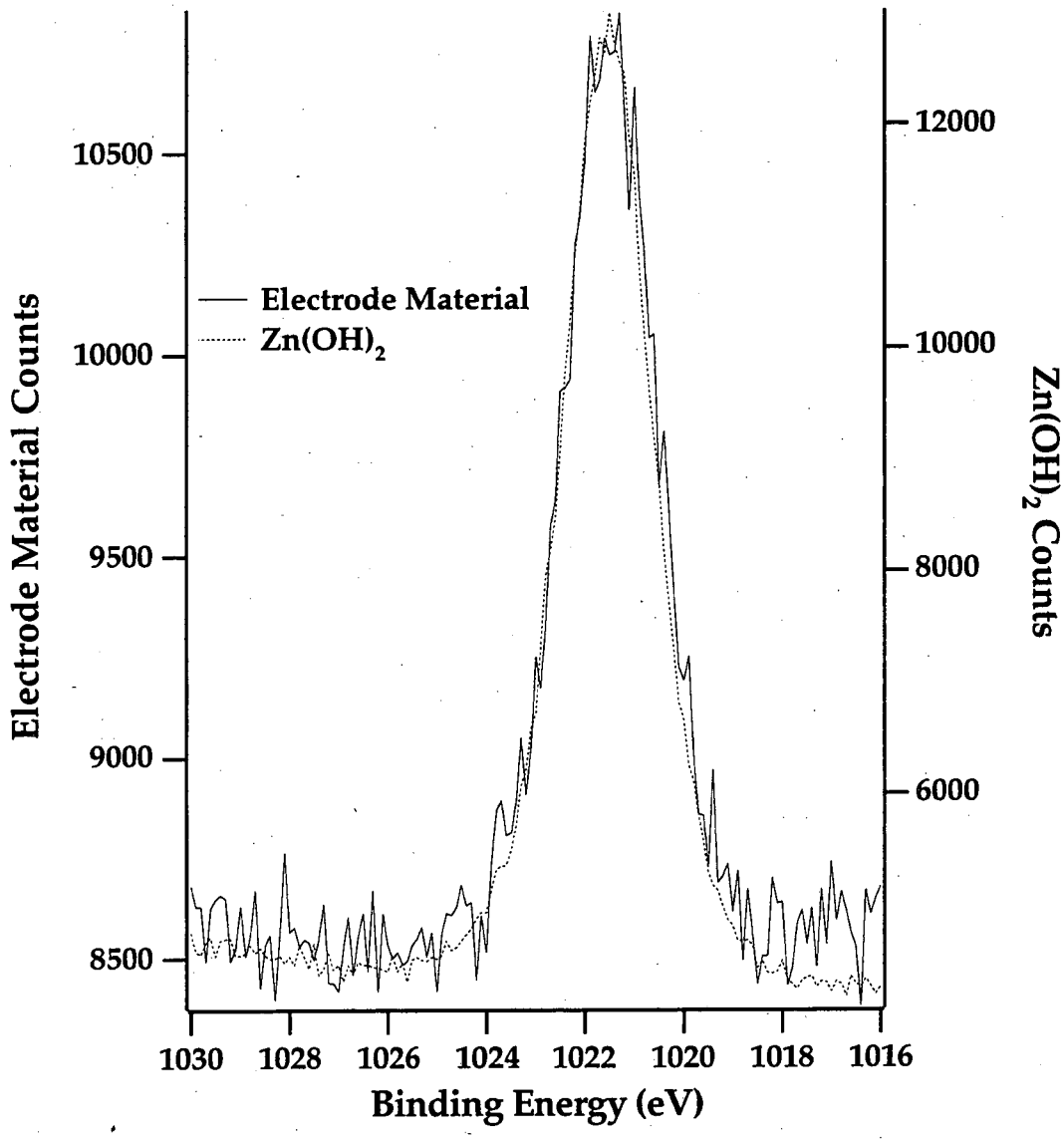

Figure 4.12: Zn $2p_{3/2}$ spectra of nickel electrode material cycled carbonate electrolyte and $Zn(OH)_2$

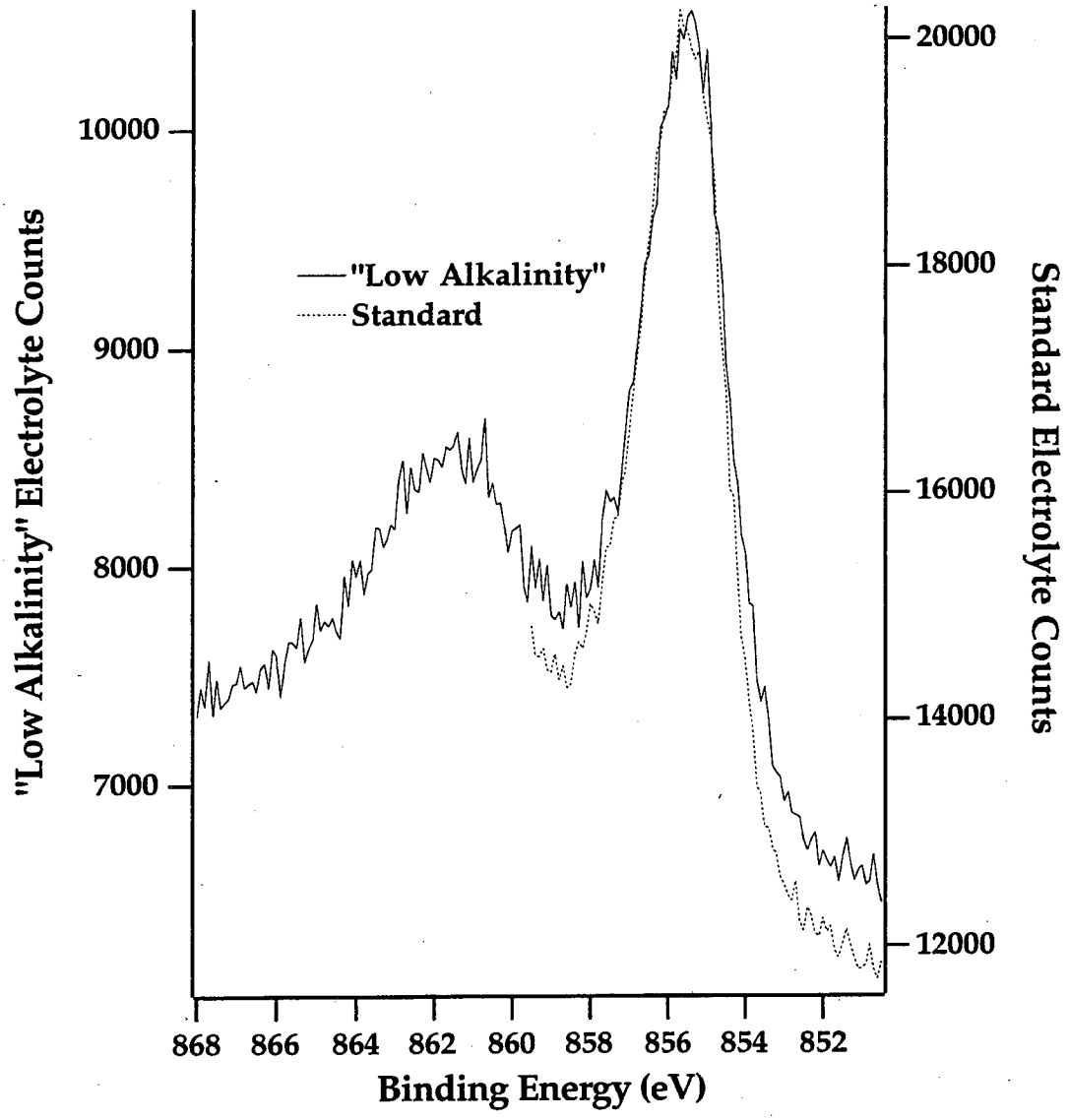

Figure 4.13: Ni $2p_{3/2}$ spectra of nickel electrode material cycled in reduced alkalinity electrolyte and in standard electrolyte

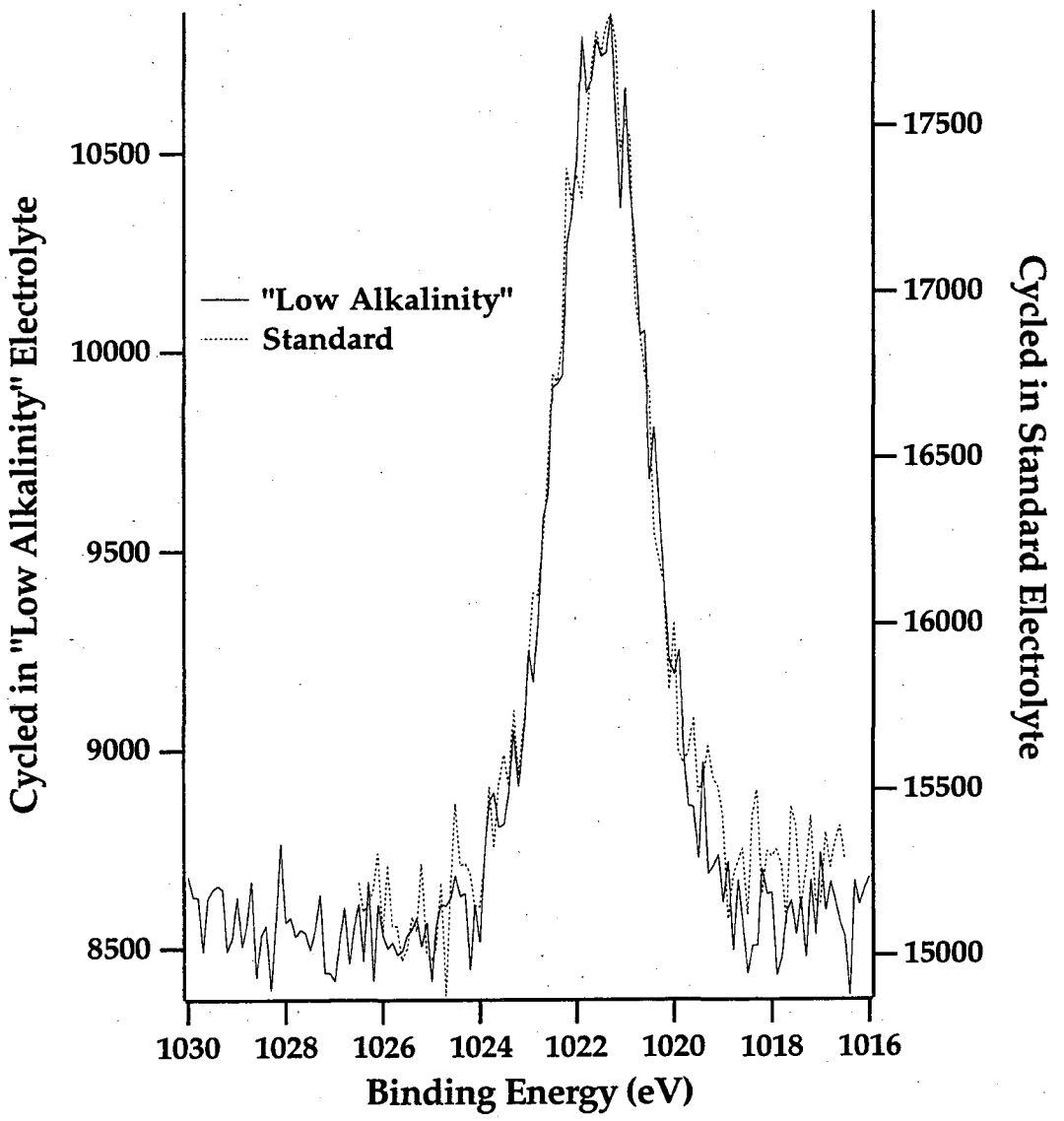

Figure 4.14: Zn $2p_{3/2}$ spectra of nickel electrode material cycled reduced alkalinity electrolyte and in standard electrolyte

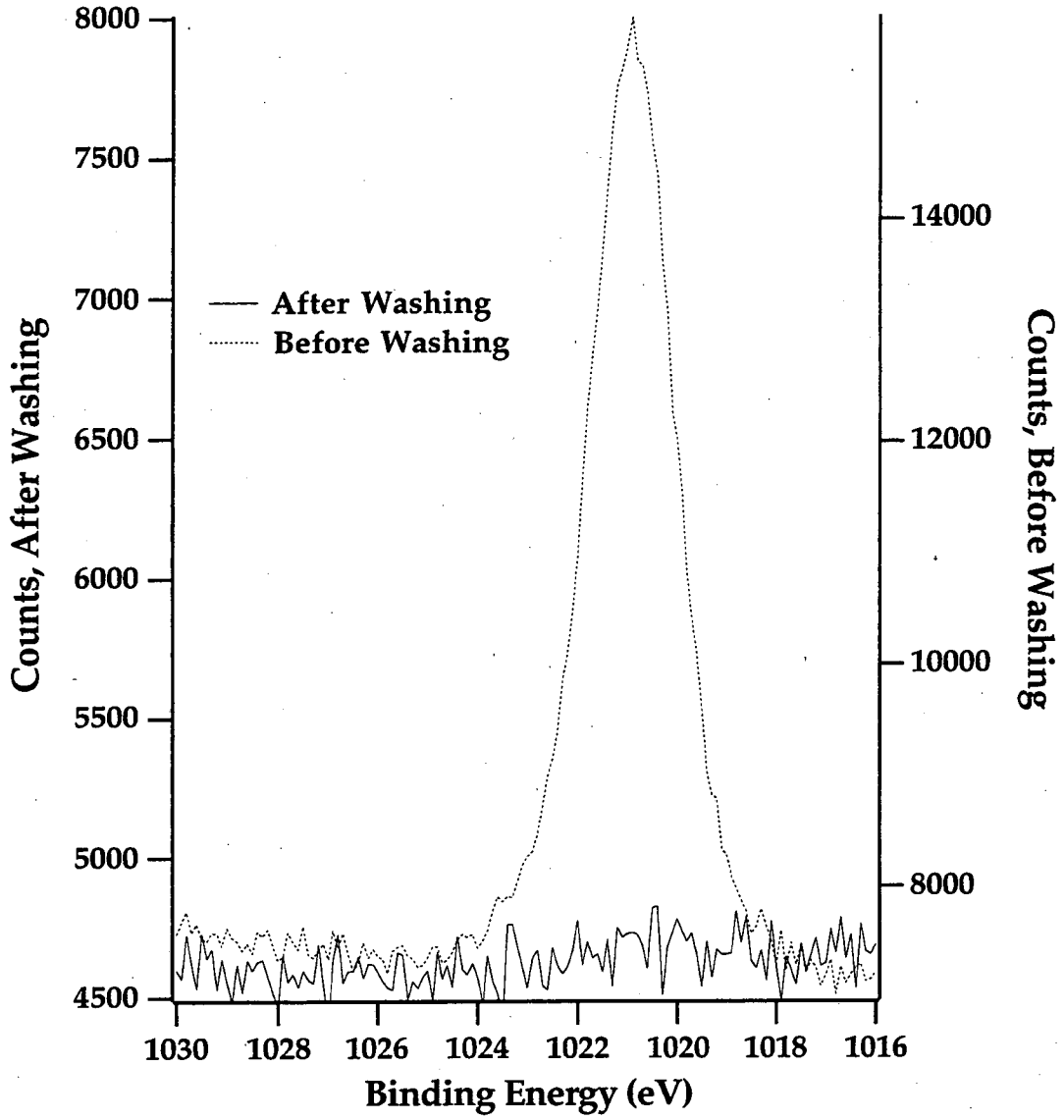

Figure 4.15: Zn $2p_{3/2}$ spectra of a nickel hydroxyzincate before and after washing in hot KOH

was repeated with electrode material that was cycled in the reduced alkalinity electrolyte.

The result is much the same, as Figure 4.16 indicates. This figure also demonstrates that the Zn species will not be removed by merely allowing it to remain in the reduced alkalinity electrolyte at room temperature, a result that will prove useful in the galvanostatic studies.

Interpretation of XPS results

There are several points that need to be made concerning the interpretation of these results. In this work, it was decided to rely more upon comparing and matching standard materials instead of relying on absolute binding energies. This was done for several reasons. First, there is the question of background removal. In the Ni $2p_{3/2}$ region, the background is highly nonlinear, as the figures in this chapter would indicate. There are many algorithms available to subtract the background, and deconvolute the data, but the issue is by no means settled and is still the subject of ongoing research. XPS Ni $2p_{3/2}$ spectra of β–$Ni(OH)_2$ have been reported by several workers [56, 57, 58, 59, 60, 61]. As Table 4.3 would indicate, there is some "spread" in the reported values. In some cases, the method of background subtraction and/or deconvolution was not reported. In others, the method of preparation and characterization of the nickel hydroxides and nickel oxyhydroxides was not reported. Thus, the safest and simplest method of characterization was the visual comparision of the spectra of standard materials prepared by known synthetic routes with the unknown materials.

A second issue is the method of charge correction. The use of adventitious carbon as a method of charge referencing is frowned upon by

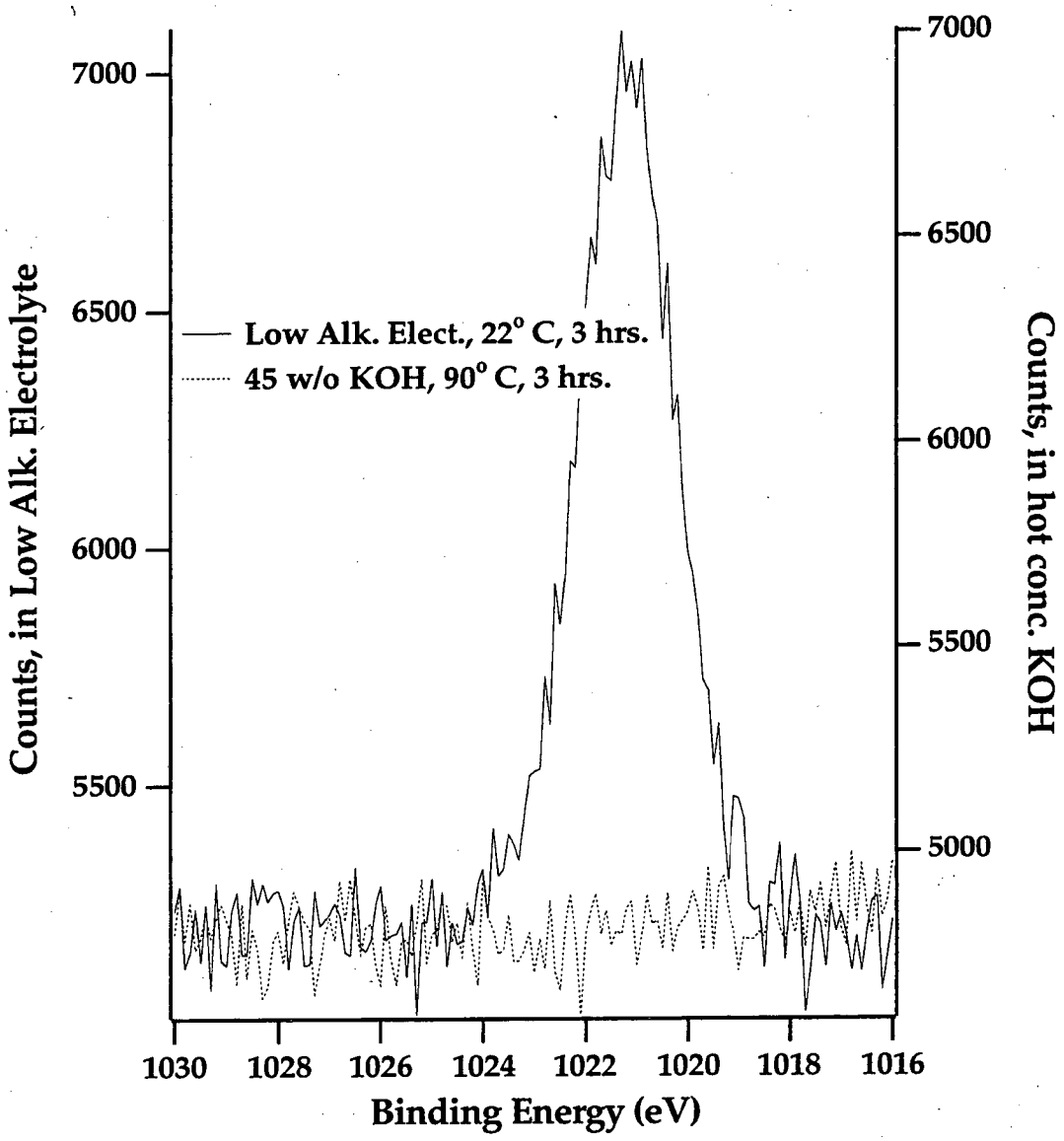

Figure 4.16: Zn $2p_{3/2}$ spectra of nickel electrode material cycled in reduced alkalinity electrolyte, before and after washing in hot KOH

Table 4.3: Reported Ni $2p_{3/2}$ binding energies for β–$Ni(OH)_2$

Binding Energy	Reference
856.6	56
855.3	57
856.45	58
856.6	59
855.8	60
855.9	61
855.3	This Work

some workers [53], but others have shown it to be a reproducible method [52]. The use of the so-called Auger parameter, α, is recommended by some workers as a reliable method of charge correction [53]. The Auger parameter is defined as:

$$\alpha = \text{K. E. of an Auger peak} + \text{K. E. of a photoelectron peak}$$

This is essentially the difference in apparent binding energies of an Auger peak and a photoelectron peak. By taking the difference between two peaks, charging effects, if constant throughout the entire binding energy range, will presumably cancel out. An Auger peak is used in the Auger parameter since in some situations, a greater shift in Auger peaks will be observed than in photoelectron peaks, making it easier to resolve two unknowns. This approach was not used here, since the Auger peaks tended to be quite broad (FWHM of about 5 eV), and non-Gaussian in

shape. In this case, reliable estimates of the Auger peak position and the Auger parameter are difficult to obtain.

Another concern is the stability of these hydrated nickel and zinc oxides under ultra-high vacuum. The various nickel oxides of interest differ substantially in their degrees of hydration, which affects their crystal structure, and possibly their response under XPS. Linn, et al. studied water adsorption and desorption from nickel hydroxide and nickel oxyhydroxide and found them to be relatively stable with regard to their XPS spectra at room temperature [62]. Still, this objection should not be overlooked.

To summarize the chemical characterization just presented, nickel oxide electrode materials and standard materials were examined by XPS. Cycled electrode materials yielded spectra that were consistent with the spectra of $Ni(OH)_2$ and ZnO or $Zn(OH)_2$. Nickel hydroxyzincates in two different Ni : Zn ratios were examined. At a high Ni : Zn ratio (10 : 1), such as would exist in a cycled nickel oxide electrode in a zinc-nickel oxide cell, the nickel hydroxyzincate yielded spectra equivalent to that of $Ni(OH)_2$ and $Zn(OH)_2$. At a lower Ni : Zn ratio (1 : 1), the results were less clear, perhaps due to charging effects. Raman spectra of this 1 : 1 material and α–$Ni(OH)_2$ were essentially identical, which would imply that the nickel hydroxyzincate exists as a co-precipitate of $Ni(OH)_2$ and a Raman-inactive form of $Zn(OH)_2$.

Resistivity measurements

The design of the zinc-nickel oxide cell pack from which samples were sectioned, and the actual cutting locations are given in Figure 4.17. Two sets of measurements were made. Figure 4.18 gives presents results of resistivity variations across selected regions of nickel electrode Ni A, whereas Figure 4.19 shows variations in resistivity through the cell pack at a selected location, the lower left corner. The resistivity of uncycled 0.46 mm (18 mil) thick sintered nickel electrodes of the type examined here was found to be 7×10^{-5} Ω–cm while that of the 0.94 mm (37 mil) thick electrodes was 18×10^{-5} Ω–cm.

As Figure 4.18 shows, there is some resistivity increase in the 0.46 mm thick electrode Ni A. There appears to be, in general, a smoothly varying resistivity. This result is interesting, in that other results [19, 20] documenting resistivity increases in cycled nickel eletrodes were referring to bulk resistivity of an entire electrode, and not a resistivity "profile".

There also appears to be a variation of resistivity with position through the cell pack, as shown in Figure 4.19. The effect seems to be more pronounced (on a relative basis) in the thicker 0.94 mm electrodes. This result has been predicted with numerical modeling [21] and has been observed previously [20] in cadmium-nickel oxide systems. There was evidence of blistering in sample Ni C, which may account for the large magnitude and erratic nature of the resistivity changes observed.

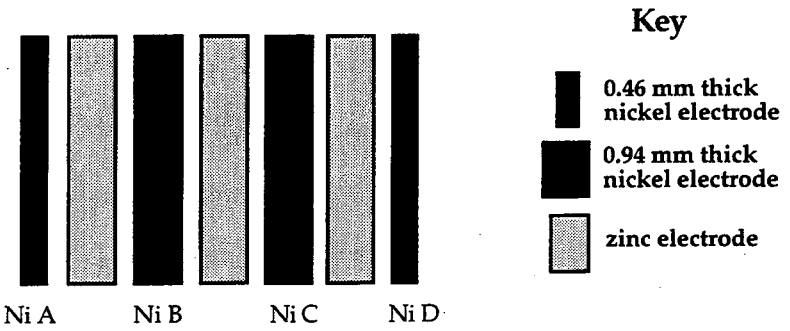

Design of cell pack

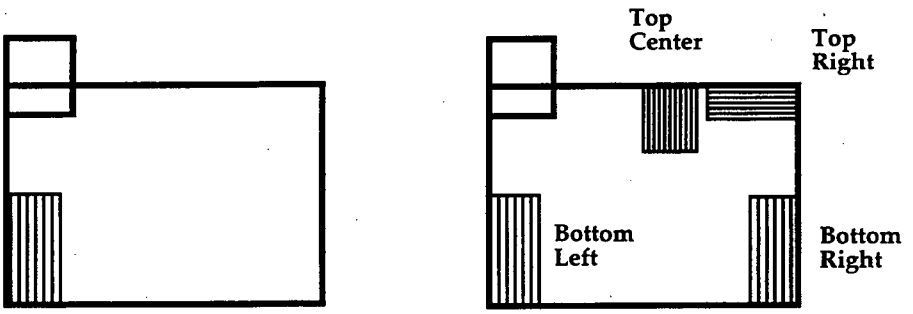

Meaurement of resistivity on all Ni electrodes through cell pack

Measurement of resistivity with position on electrode Ni A

Figure 4.17: Cell configuration, and sampling locations for resistivity measurements.

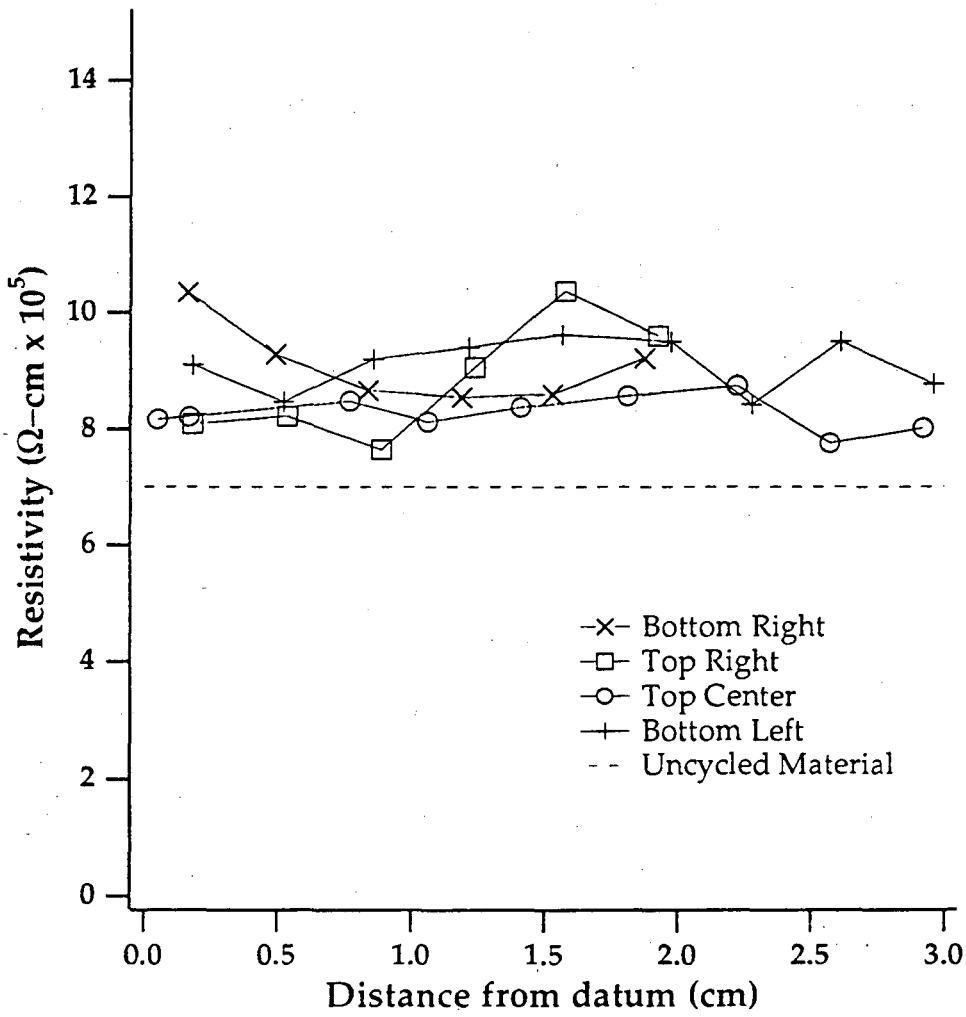

Figure 4.18: Resistivity variation of nickel electrode Ni A at four locations.

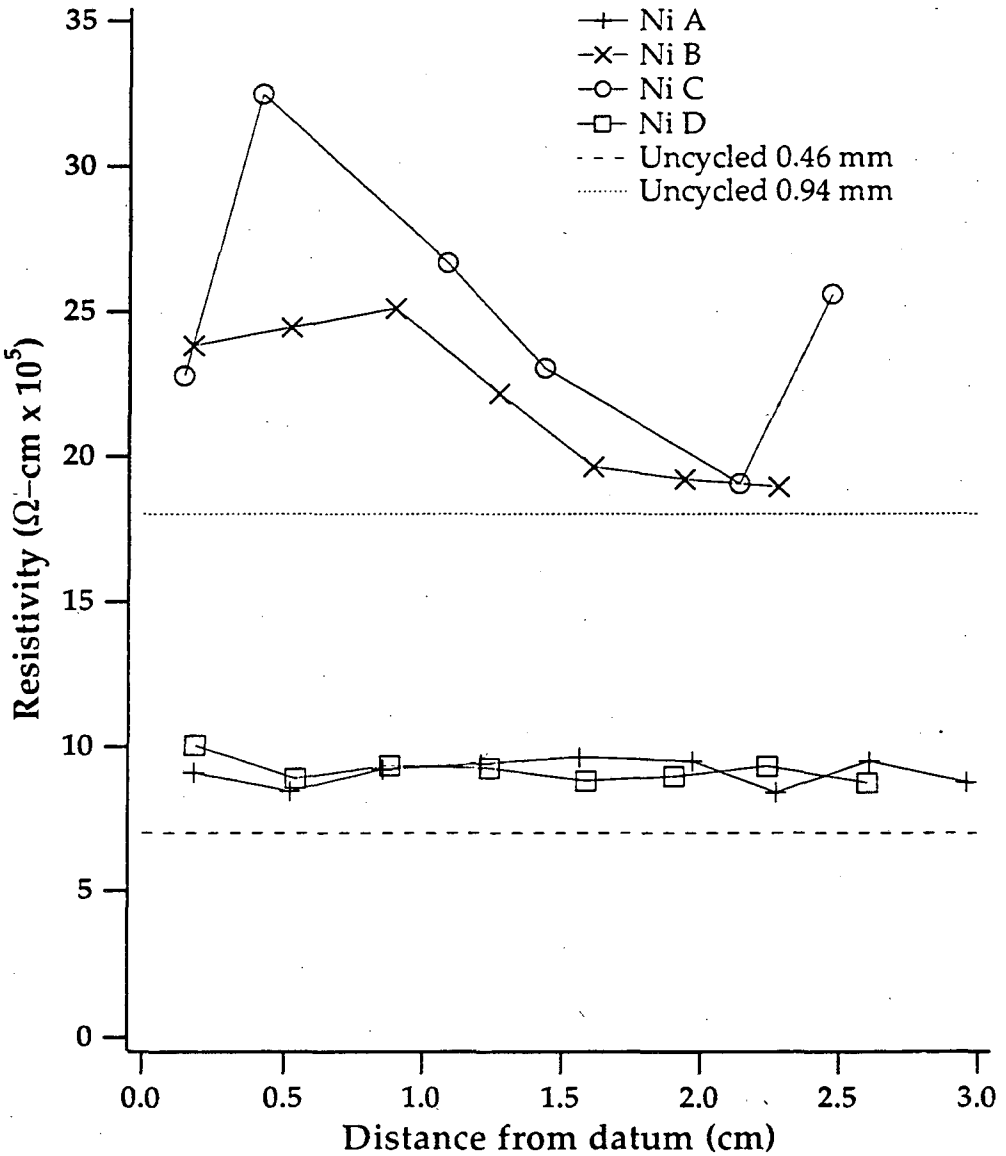

Figure 4.19: Resistivity variation of nickel electrodes through the cell pack.

Optical microscopy

Optical microscopy was used to examine large-scale structural changes in the electrode materials. In general, there was visible evidence of delamination behavior in electrode materials that exhibited the greatest capacity loss. Figure 4.20 is a cross-sectional view of uncycled nickel oxide electrode material. Figure 4.21 displays the cross-section of material that has been cycled. The cycled material was taken from electrode Ni C and prepared as referred to in the section on resistivity measurements. Magnification in the photographs is about 400x; the width of the electrodes is 0.94 mm.

One can note the relatively large fissures beginning near the wires of the nickel mesh, extending in a planar fashion throughout the electrode. Among others, Fritts also observed this behavior, and speculated that it may be the precursor to blistering [20].

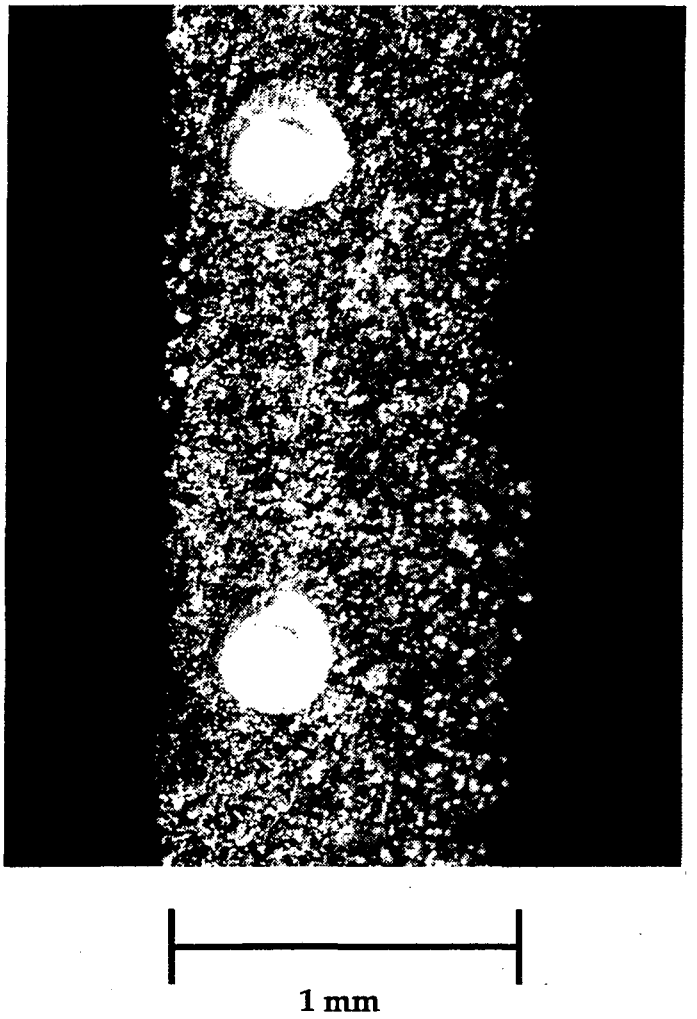

Figure 4.20: Optical micrograph of uncycled nickel electrode material.

Figure 4.21: Optical micrograph of cycled nickel electrode material.

Cell cycling results

As outlined in Chapter III, the goal of the cell cycling experiments was to determine, through a series of modifications in the operating conditions, whether a significant part of lost capacity could be recovered. Table 3.2 contains a summary of the operating conditions. Briefly, all runs were conducted in 5.9 M KOH and 1.1 M LiOH, with ZnO added to saturation. Modifying treatments included addition of surfactant to the electrolyte, washing of the electrode in KOH, and compression of the electrode.

Figure 4.22 compares the charge/discharge behavior of the electrode without any modifications (A) to cycles with the addition of Triton X-100 in concentrations of 370 mg/L (B) and 1100 mg/L (C1 and C2). The cells were charged at a C/6 rate (current density of 5.33 mA/cm^2) with constant-voltage limited charging beginning at 530 mV versus a Hg/HgO reference electrode in the same electrolyte. The discharge was at a C/6 rate. As the figure shows, there is a small positive effect when adding a surfactant to the electrolyte, although a large increase in the concentration does not seem to bring additional benefits. One should also note the small variability of discharge capacity from cycle to cycle within a given run (e.g. C1 and C2). These variations have been observed earlier in nickel electrodes in zinc-nickel oxide cells that have lost capacity during cycling [28].

The effect of washing the electrode on discharge capacity is shown in Figure 4.23. To gain an indication of the rate dependence as well, the electrode was charged and discharged more slowly in this case. Charging was at a C/15 rate (current density of 2.13 mA/cm^2), with a constant-voltage charging beginning at 530 mV. Discharge was at the C/15 rate.

One can note that the change in capacity when cycled in an electrolyte containing 370 mg/L Triton X-100 before washing (B) versus the capacity in the same electrolyte after washing (D) is very slight. This is in contrast to the result of Dmitrenko, et al. [25], who claimed that by washing in hot KOH, a recovery in failed nickel electrodes used in zinc-nickel oxide cells could be attained. It should be noted that their system used simply a KOH/LiOH electrolyte, and not the KOH/LiOH/CO_3^{2-}/F^- system studied here. Details of the extent and method of capacity recovery were sparse as well.

Mechanical compression of the electrodes was also attempted to recover capacity. In Figure 4.24, results for cycling runs under compression of 310 kN/m^2 (E), 675 kN/m^2 (F), and 2070 kN/m^2 (G) are shown. The application of pressure does not seem to influence the discharge capacity a great deal, indicating that contact with isolated portions of the electrode cannot be reestablished in this way.

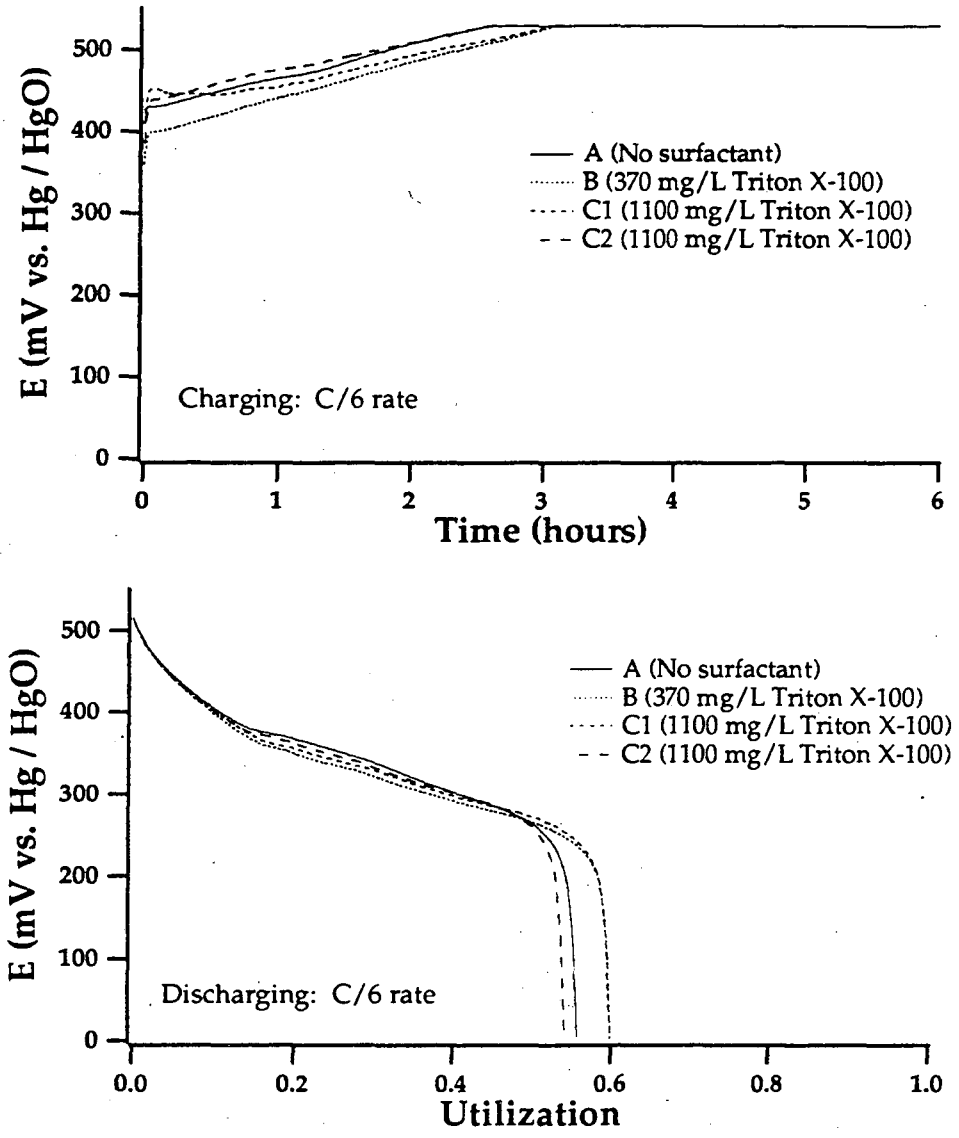

Figure 4.22: Influence of surfactant concentration on discharge capacity. Charging is at the C/6 rate with a constant-voltage taper at 530 mV. Discharge is at the C/6 rate with a cutoff at 0 mV.

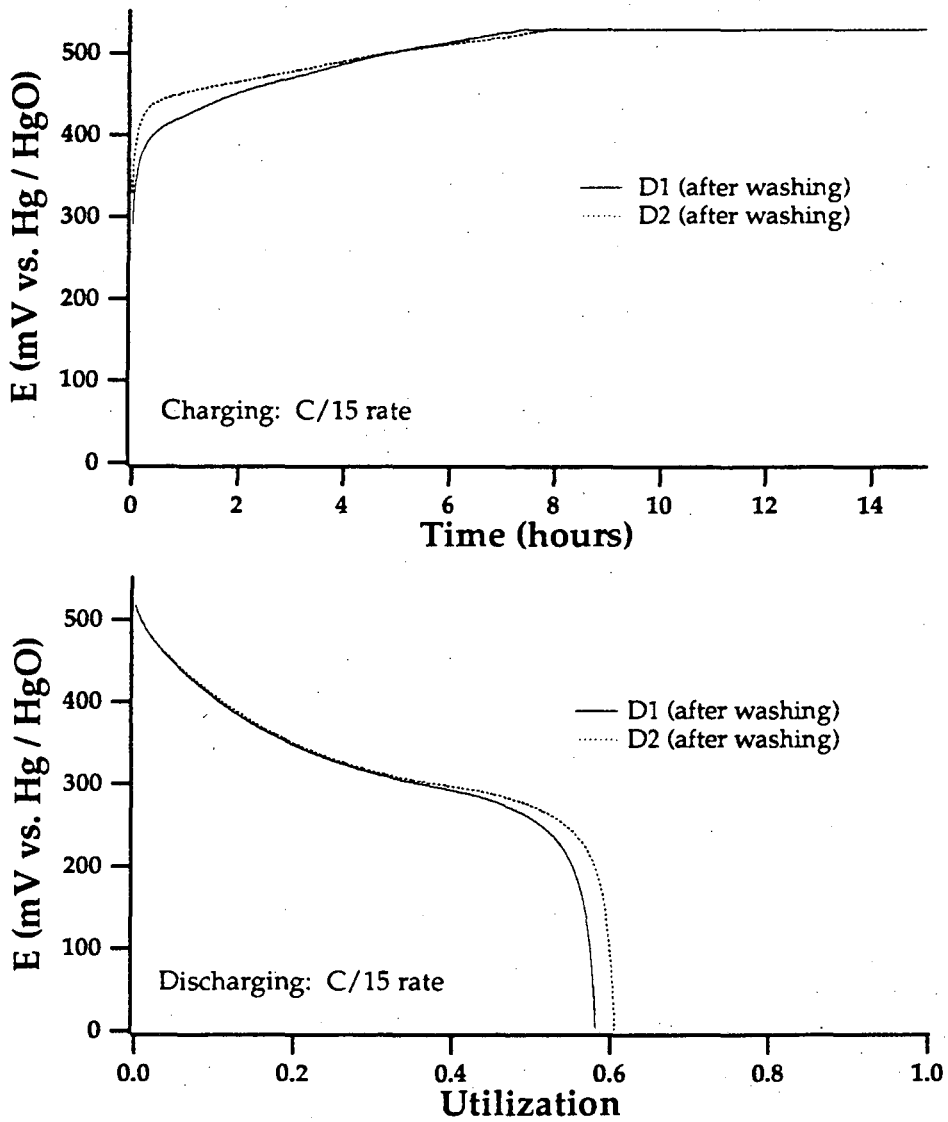

Figure 4.23: Effect of washing on discharge capacity.
Charging is at the C/15 rate with a constant-voltage taper at 530 mV.
Discharge is at the C/15 rate with a cutoff at 0 mV.

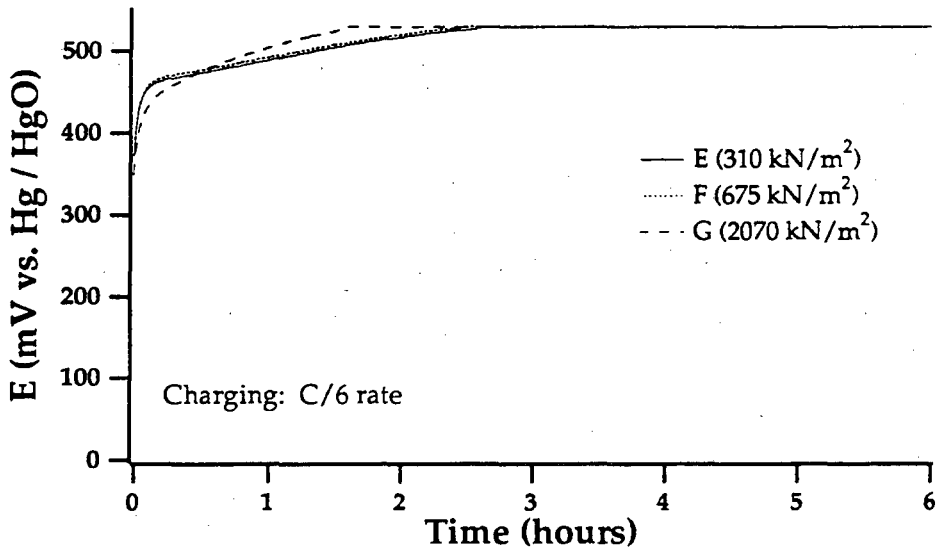

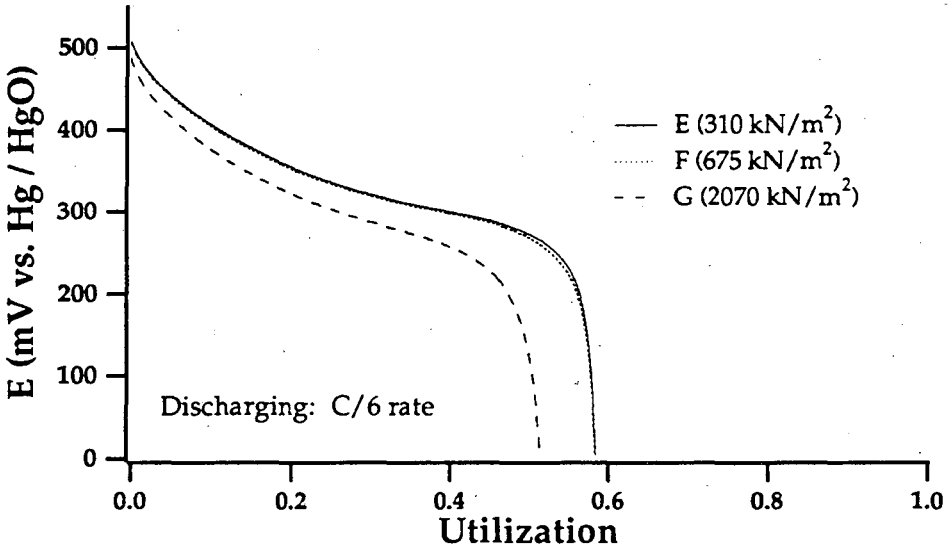

Figure 4.24: Effect of compression on discharge capacity.

Charging is at the C/6 rate with a constant-voltage taper at 530 mV. Discharge is at the C/6 rate with a cutoff at 0 mV.

Chapter V: Conclusions and Recommendations

In this work, nickel oxide electrodes that were cycled to failure in zinc-nickel oxide cells were characterized. These cells incorporated novel electrolytes that were intended to increase the cycle life of the zinc electrode. An important question was the nature of the zinc species that was found to be deposited in the failed nickel electrodes. Photoelectron spectroscopy indicated that the form of zinc is probably $Zn(OH)_2$ or ZnO. There have been reports in the literature that a nickel - zinc compound, "nickel hydroxyzincate", may be responsible for the capacity degradation of nickel oxide electrodes in zinc-nickel oxide cells. Several methods were used to characterize this material, including photoelectron spectroscopy, Raman spectroscopy, and x-ray diffraction. The results obtained, while not fully definitive, suggest that the characterization of this material as a compound in the sense of having nickel and zinc present in the same crystal lattice may not be correct. A better interpretation is that the material probably exists as a co-precipitate, or perhaps as an intercalation compound, with zinc species existing between the sheets of turbostratic nickel hydroxide. Evidence of a more convincing nature could be obtained through EXAFS measurements.

Considerable evidence was found for a strictly mechanical interpretation of the capacity degradation of the nickel oxide electrodes studied. The resistivity of cycled electrodes is substantially greater than that of uncycled ones. This increase is significant in that it implies that some active material may be losing electrical contact with the electrode, leading to a decrease in observed discharge capacity. Spatial variations of the resistivity increase were also recorded. Optical microscopy confirmed the presence of

extensive mechanical degradation within some cycled electrode samples. Cell cycling experiments did not suggest that the capacity loss is due to a loss of wetting, although experiments conducted with a surfactant were not exhaustive. Attempts to wash the electrode to remove precipitated zinc species, a strategy which has been reported to work in some zinc-nickel oxide experiments, were found to have little effect. Compression of cycled nickel oxide electrodes, in an attempt to improve electrical contact between the active material and the current collector, was also found to yield little improvement. In summary, the capacity degradation of nickel oxide electrodes in zinc-nickel oxide cells, when using novel, low-alkalinity electrolytes, seems to be largely mechanical in nature, and irreversible. If this interpretation of the degradation of the nickel electrode is correct, then the use of thinner electrode materials and a stronger nickel sinter according to Fritts [19,20] and Lanzi and Landau [21] may lead to improvement of the cycle life performance of this zinc-nickel oxide system. Such a strategy would probably lead to a decrease in the specific energy and specific power of the cell, which is undesirable for applications requiring a high specific energy. Another question that needs to be examined more closely is the role of zinc compounds, if any, in accelerating the observed mechanical damage of the nickel electrode.

Among the other issues that merit further attention is the importance of gas evolution in the failure of nickel electrodes in the zinc-nickel oxide system when using a reduced-alkalinity electrolyte. Adler, et. al. [28] report that a certain degree of oxygen evolution on charge is beneficial because the oxygen oxidizes zinc dendrites which may short the cell. A primary component of the reduced-alkalinity electrolytes studied was carbonate,

which enhances oxygen evolution on nickel [37]. Fritts [19,20] reports, however, that gas evolution will lead to damage of the sintered nickel electrode material, leading to a decline in the capacity of the electrode. The possibliity exists to perhaps optimize the charging of the nickel electrode to supply enough oxygen to eliminate dendritic shorting, while at the same time minimizing mechanical damage due to gas evolution. Since the physics of electrolytic gas evolution is complex, such optimization would probably be best attempted experimentally.

Appendix: Preparation and Characterization of Reference Compounds

Several compounds were prepared according to standard literature methods. This was done instead of producing the various nickel phases electrochemically so that one could have well-defined, reproducible reference phases. All water used in the syntheses was Millipore high-resistivity water, with ρ = 15 Mσ-cm or better. X-ray diffraction patterns of the compounds tested are included as Figures A.1 to A.7. The x-ray diffraction unit (Siemens) was operated using Cu Kα radiation. Scan ranges are as indicated on the figures, with a step size of 0.1 degree and a time increment of 1.0 second per step.

<u>β–$Ni(OH)_2$</u>

This material was obtained from Inco, Ltd. The x-ray diffraction, shown as Figure A.1, agrees well with JCPDS pattern 14-0117, synonym theophrastite.

<u>α–$Ni(OH)_2$</u>

This phase was prepared according to the method of Faure, et. al [8]. To 50 mL of an aqueous solution 1.0 M in $Ni(NO_3)_2 \bullet 6\ H_2O$ (Mallinckrodt, AR grade), 5.5 mL concentrated (27 w/o), aqueous NH_4OH solution (Mallinckrodt, AR grade) was added dropwise. The mixture was stirred at room temperature for four hours. The precipitate was then washed with several portions of water then a final rinse with acetone (J. T. Baker, "Baker Analyzed" grade), and allowed to dry. The x-ray diffraction pattern, given as Figure A.2, agrees with those published by Faure, et. al.

β–NiOOH

This phase was produced according to the method of Glemser [5]. A solution of 3.83 g $Ni(NO_3)_2 \bullet 6\ H_2O$ in 50 mL water was added dropwise to a solution consisting of 1.03 g KOH pellets (J. T. Baker, "Baker Analyzed" grade), and 0.4 mL Br_2 (Mallinckrodt, AR grade) in 10 mL H_2O. A black precipitate appeared. The precipitate was immediately washed with two 750 mL portions of water followed by five 250 mL portions of water. The wet precipitate was then stored under concentrated H_2SO_4 for two weeks. The x-ray diffraction pattern, given in Figure A.3, matches that published by Faure, et. al [8], who used a similar synthetic route.

Nickel hydroxyzincates

These were produced according to the nearly-identical methods of Bode [6] and Romanov [26], and are analagous to the method of Faure, et. al [8] for the production of α-$Ni(OH)_2$ For the 10: 1 nickel -zinc ratio material, a 50 mL solution containing 1.0 M $Ni(NO_3)_2 \bullet 6\ H_2O$ and 0.1 M $Zn(NO_3)_2 \bullet 6\ H_2O$ (J. T. Baker, "Baker Analyzed" grade) was prepared. To this was added 5.5 mL of concentrated NH_4OH solution. The mixture was stirred for four hours at room temperature. Final washing steps were similar to that of the preparation of α–$Ni(OH)_2$. Preparation of the 1:1 nickel - zinc ratio material was identical to the 10:1 compound, except that the starting solution was 1.0 M in $Zn(NO_3)_2 \bullet 6\ H_2O$ instead of 0.1 M. The x-ray diffraction patterns, given in Figures A.4 and A.5, are nearly identical to that of α–$Ni(OH)_2$, as was reported by Bode [6].

$Zn(OH)_2$

This material was purchased from Alfa. The x-ray diffraction pattern, given as Figure A.6, matches JCPDS file 12-0479, synonym wulfingite.

ZnO

This material was purchased from Aldrich (99.999%). The x-ray diffraction pattern, given as Figure A.7, matches that of JCPDS file 05-0664, synonym zincite.

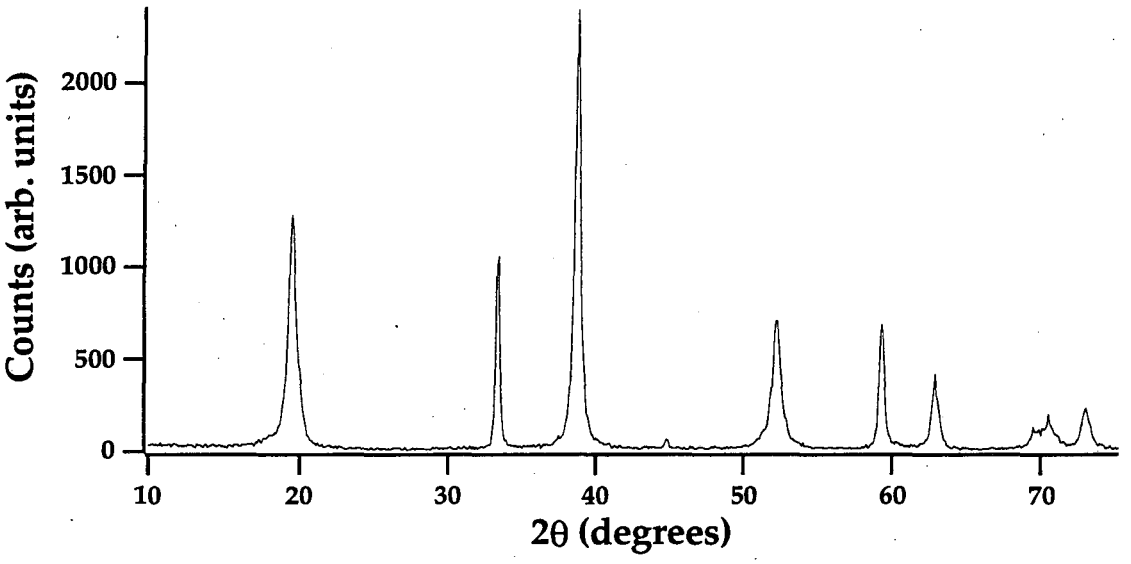

Figure A.1: X-ray diffraction pattern of β–$Ni(OH)_2$

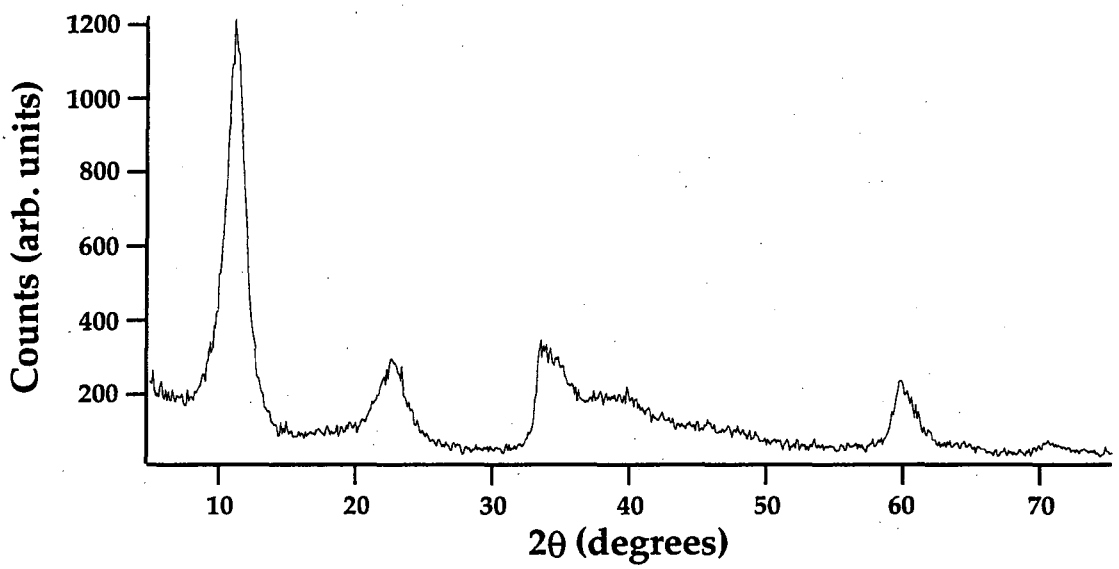

Figure A.2: X-ray diffraction pattern of α–$Ni(OH)_2$

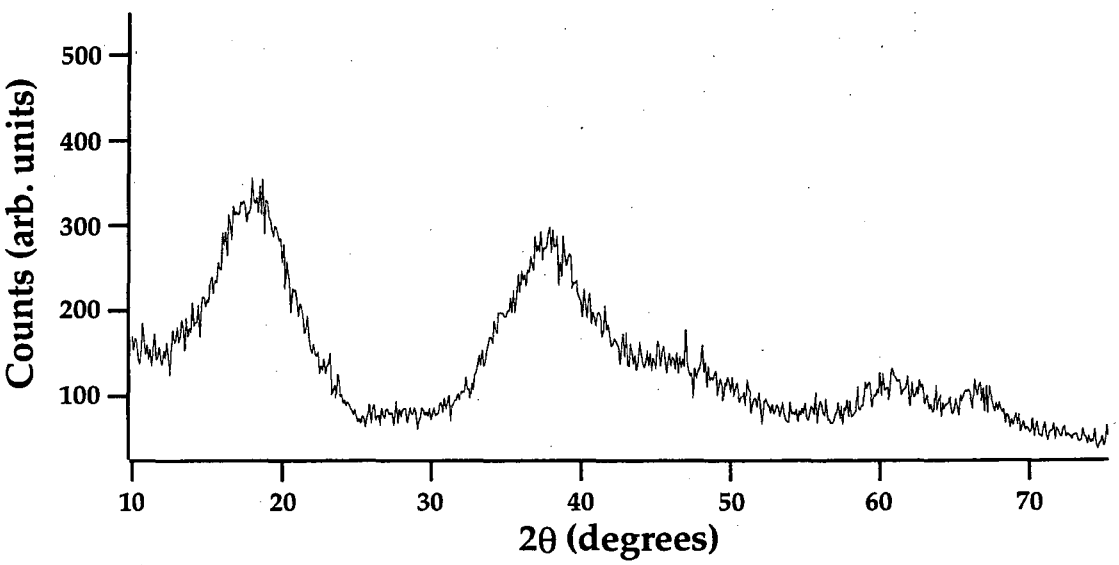

Figure A.3: X-ray diffraction pattern of β–NiOOH

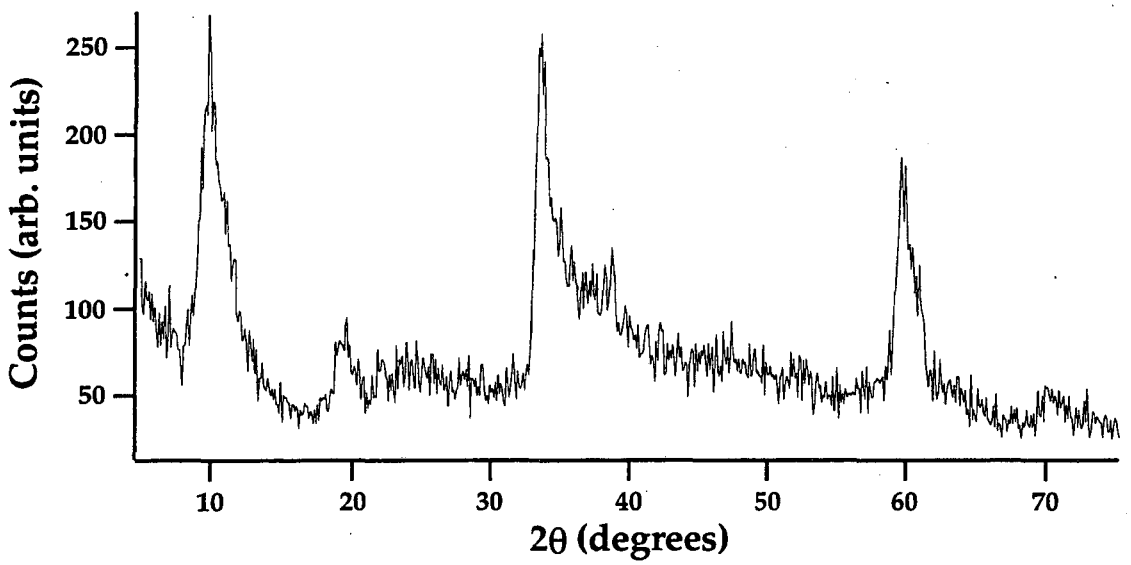

Figure A.4: X-ray diffraction pattern of a nickel hydroxyzincate with a nickel-zinc ratio of 1:1

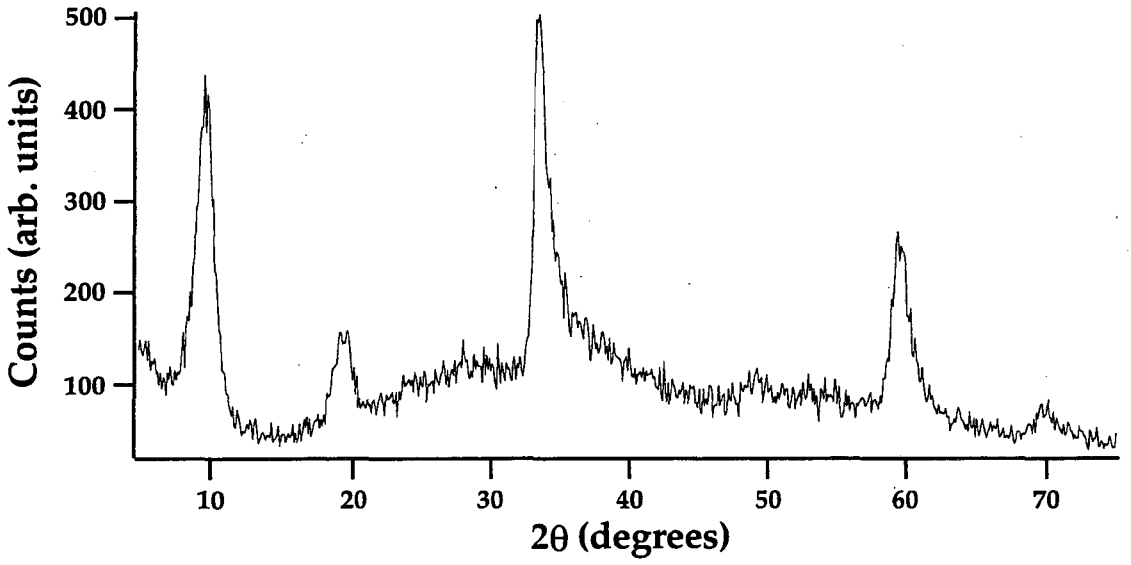

Figure A.5: X-ray diffraction pattern of a nickel hydroxyzincate with a nickel-zinc ratio of 10:1

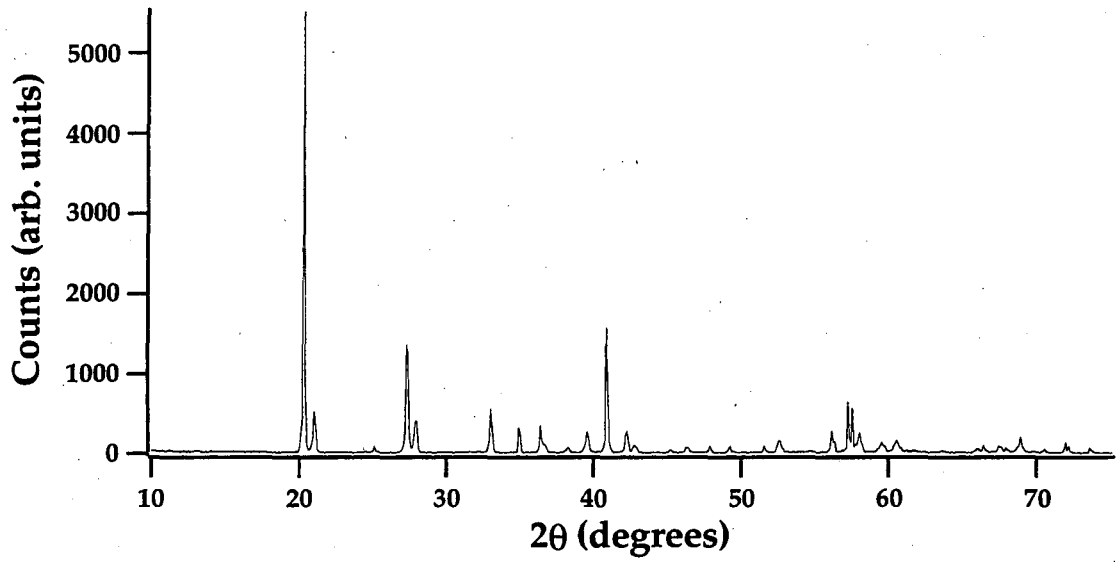

Figure A.6: X-ray diffraction pattern of $Zn(OH)_2$

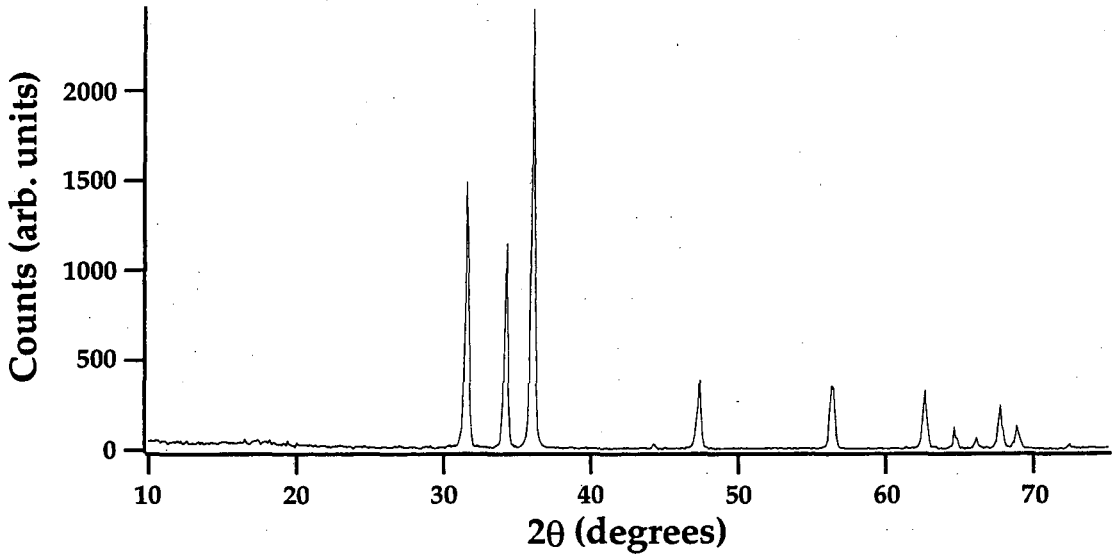

Figure A.7: X-ray diffraction pattern of ZnO

Bibliography

1. D.F. Gosdes, *J. Power Sources*, **45**, 61 (1993).

2. J.H.B. George, "The World Battery Industry. A Multiclient Study.," George Consulting International, 1989.

3. F.R. McLarnon, personal communication, Berkeley, CA, Aug. 1993.

4. E.J. Cairns and F.R. McLarnon, in **Proc. Symp. on Batteries and Fuel Cells for Stationary and Electric Vehicle Applications**, A.R. Landgrebe and Z. Takehara, eds., The Electrochemical Society, Pennington, NJ, 1993, pp. 1-11.

5. O. Glemser and J. Einerhand, *Zeit. fur anorg. Chem.*, **261**, 27 (1950).

6. H. Bode, K. Dehmelt, and J. Witte, *Electrochim. Acta*, **11**, 1079 (1966).

7. J. McBreen in **Modern Aspects of Electrochemistry**, Plenum Press, R.E. White, J.O.M. Bockris, and B.E. Conway, eds., New York, 1989, pp. 29.

8. C. Faure, C. Delmas, and M.J. Fouassier, *J. Power Sources*, **35**, 279 (1991).

9. P. Oliva, J. Leonardi, J.F. Laurent, C. Delmas, J.J. Braconniier, M. Figlarz, F. Fievet, and A. de Guibert, *J. Power Sources*, **17**, 589 (1982).

10. A. Delahaye-Vidal and M. Figlarz, *J. Applied Electrochem.*, **17**, 589 (1987).

11. M. Paszkiewick, *J. Appl. Electrochem.*, **11**, 135 (1981).

12. A. Fleischer, *Trans. Electrochem. Soc.*, **94**, 289 (1948).

13. P.Y. Lu, in **Proc. Symp. Adv. Battery Materials and Processes**, The Electrochemical Society, Pennington, NJ, 1984, pp. 218.

14. E. Buder, *J. Applied Electrochem.*, **2**, 301 (1972).

15. I. Arulraj and D.C. Trivedi, *Int. J. Hydrogen Energy*, **14**, 893 (1989).

16. B.E. Conway, M.A. Sattar, and D. Gilroy, *Electrochim. Acta*, **25**, 973 (1980).

17. G. Bronoel and J. Reby, *Electrochim. Acta*, **25**, 973 (1980).

18. K. Kinoshita, "Electrochemical Oxygen Technology", John Wiley & Sons, New York, (1992).

19. D.H. Fritts, *J. Power Sources*, **6**, 327 (1981).

20. D.H. Fritts, *J. Power Sources*, **12**, 267 (1984).

21. O. Lanzi and U. Landau, *J. Electrochem. Soc.*, **138**, 2527 (1991).

22. M. Natan, D. Belanger, M. Carpenter, and M. Wrighton, *J. Phys. Chem.*, **91**, 1834 (1987).

23. A. Briggs, *J. Applied Electrochem.*, **21**, 999 (1982).

24. V. Dmitrenko, M. Zubov, V. Barsukov, and L. Sagoyan, *Elektrokhimiya*, **23**, 1240 (1987).

25. V. Dmitrenko, M. Zubov, V. Baulov, L. Sagoyan, and V. Barsukov, *Elektrokhimiya*, **19**, 852 (1983).

26. V. Romanov, *Zh. Priklad. Khim.*, **34**, 1317 (1961).

27. V. Kozyrin, A. Bachaev, S. Bazarov, and V. Flerov, *Elektrokhimiya*, **25**, 267 (1989).

28. T.C. Adler, F.R. McLarnon, and E.J. Cairns, *J. Electrochem. Soc.*, **140**, 289 (1993).

29. V. Gud, V. Nikol'skii, Z. Arkhangel'skaya, and G. Reshetova, *Zh. Priklad. Khim.*, **63**, 2650 (1990).

30. A. Zimmerman and P. Effa, *J. Electrochem. Soc.*, **131**, 709 (1984).

31. A. Sood, *J. Applied Electrochem.*, **16**, 274 (1986).

32. G.P. Kalaignan, V. Muralidharan, and K. Vasu, *Indian J. Technol.*, **16**, 518 (1989).

33. M.E. Unates, M.E. Folquer, J.R. Vilche, and A.J. Arvia, *J. Electrochem. Soc.*, **135**, 25 (1988).

34. K. Vasu, V. Muralidharan, M. Ramakrishna, G.P. Kalaignan, and N. Jaylakshmi, *J. Power Sources*, **28**, 409 (1989).

35. P.V. Kamath and M.F. Ahmed, *J. Applied Electrochem.*, **23**, 225 (1993).

36. B. Ezhov and O. Malandin, *J. Electrochem. Soc.*, **138**, 885 (1991).

37. V. Muralidharan, N. Jayalakshmi, and P. Mageswari, *Bull. of Electrochem.*, **7**, 355 (1991).

38. F.R. McLarnon and E.J. Cairns, *J. Electrochem. Soc.*, **138**, 645 (1991).

39. T.P. Dirkse in **IUPAC Solubility Data Series**, McGraw-Hill, 1986.

40. T. Katan, J. Savory, and J. Perkins, *J. Electrochem. Soc.*, **126**, 1835 (1979).

41. C. Debiemme-Chouvy and J. Vedel, *J. Electrochem. Soc.*, **138**, 2538 (1991).

42. J. McBreen and E. Cairns in **Adv. Electrochem. Electrochem. Engr.**, H. Gerischer and C. Tobias eds., McGraw-Hill, 1978, pp. 273.

43. J.S. Chen, F.R. McLarnon, and E.J. Cairns, *J. Power Sources*, **39**, 333 (1992).

44. R. Jain, T.C. Adler, F.R. McLarnon, and E.J. Cairns, *J. Appl. Electrochem.*, **22**, 1039 (1992).

45. R.F. Thornton and E.J. Carlson, *J. Electrochem. Soc.*, **127**, 1448 (1980).

46. J.T. Nichols, F.R. McLarnon, and E.J. Cairns, *Chem. Eng. Commun.*, **38**, 357 (1985).

47. M.Eisenberg, (Electrochimica Co.), *U.S. Pat. 4,224,391* (1980).

48. D. Reisner and M. Eisenberg, in **Proceedings of the 24th Intersociety Energy Conversion Engineering Conference**, IEEE, 1989, pp. 1677.

49. T. Adler, unpublished data, Lawrence Berkeley Laboratory, Berkeley, CA, March 1994.

50. R. Barnard, C.F. Randall, and F.L. Tye, *J. Appl. Electrochem.*, **10**, 127 (1980).

51. D.P. Woodruff and T.A. Delchar, "Modern Techniques of Surface Science", Cambridge University Press, Cambridge, 1986.

52. C.D. Wagner, W.M. Riggs, L.E. Davis, J.F. Moulder, and G.E. Muilenberg, "Handbook of X-ray Photoelectron Spectroscopy", Physical Electronics Division, Perkin-Elmer Corporation, Eden Prarie, Minnesota, 1979.

53. "Practical Surface Analysis, Volume 1: Auger and X-ray Photoelectron Spectroscopy", D. Briggs and M.P. Seah, eds., John Wiley and Sons, Ltd., London, 1990.

54. C. Johnston and P.R. Graves, *Appl. Spectroscopy*, **44**, 105 (1990).

55. A.H.L. Goff, S. Joiret, B. Saidani, and R. Wiart, *J. Electroanal. Chem.*, **263**, 127 (1989).

56. K.S. Kim and N. Winograd, *Surf. Sci.*, **43**, 625 (1974).

57. T. Dickenson, A.F. Povey, and P.M.A. Sherwood, *J. Chem. Soc. Faraday Trans. I.*, **73**, 327 (1977).

58. T.L. Barr, *J. Phys. Chem*, **82**, 1801 (1978).

59. K.S. Kim, W.E. Baitinger, J.W. Amy, and N. Winograd, *J. Electron Spect. Rel. Phenom.*, **5**, 351 (1974).

60. B.P. Lochel and H.H. Strehblow, *J. Electrochem. Soc.*, **131**, 713 (1984).

61. N.S. McIntyre, T.E. Rummery, M.G. Cook, and D. Owen, *J. Electrochem. Soc.*, **123**, 1164 (1976).

62. J.H. Linn and W.E. Swartz, Jr., *Applic. Surf. Sci.*, **20**, 154 (1984).

LAWRENCE BERKELEY LABORATORY
UNIVERSITY OF CALIFORNIA
TECHNICAL INFORMATION DEPARTMENT
BERKELEY, CALIFORNIA 94720